npj | climate and atmospheric science

Article

Published in partnership with CECCR at King Abdulaziz University

https://doi.org/10.1038/s41612-025-01147-0

Linking North Pacific eastern subtropical mode water to ENSO: precursor signatures and subtropical cell pathways

LingLing Liu[1,2,3] ✉, Jin-Yi Yu[2] ✉, Fan Wang[1,3], Jianing Wang[1,3] & YongFu Lin[4]

Mode waters play a crucial role in ocean heat and carbon storage, as well as in climate variability. Here we reveal a strong relationship between the North Pacific Eastern Subtropical Mode Water (NPESTMW) and El Niño-Southern Oscillation (ENSO) events. NPESTMW volume anomalies exhibit significant correlations with the Ocean Niño Index up to nine months in advance. Our analysis identifies two distinct pathways connecting NPESTMW and ENSO development. First, NPESTMW serves as a footprint of the Pacific Meridional Mode, a well-established ENSO precursor. Second, NPESTMW influences tropical Pacific sea surface temperature through the Subtropical Cell. Notably, our findings indicate that stronger NPESTMW volume anomalies are more closely tied to multi-year ENSO events than to single-year development, especially for the La Niña phase. These discoveries offer new insights into the roles of subtropical mode water in shaping ENSO development.

Mode waters play a crucial role in regulating the global ocean and thus Earth's climate system by contributing to heat storage and carbon sequestration[1–5]. These unique layers of ocean stratification, characterized by vertically homogeneous properties within or above the permanent pycnocline, are primarily found in subtropical and subpolar gyres[6]. Formed mainly through wintertime deep convection, mode waters capture atmospheric conditions during their formation before being subducted into the ocean interior[7–9]. Recent studies highlight their role in enhancing heat sequestration in the deep ocean under global warming[5,10,11]. However, the potential role of mode waters as indicators or modulators of major climate phenomena is not yet fully understood.

One of the most important climate phenomena is the El Niño–Southern Oscillation (ENSO), the dominant mode of interannual variability in the global climate system[12]. ENSO exerts profound influences on ecosystem, agriculture, and extreme weather events worldwide[13–17]. Traditional ENSO dynamics emphasize equatorial Pacific processes[18]; however, a paradigm shift occurred around 1990, with ENSO's primary dynamic transitioning from the tropical to the subtropical Pacific[19]. In this subtropical Pacific ENSO dynamic, the Pacific Meridional Mode (PMM) emerges as a crucial component, originating in the northeastern Pacific and propagating sea surface temperature (SST) anomalies to the central tropical Pacific, thus facilitating ENSO development[20–23]. Despite these advances, ENSO predictability remains a considerable challenge, particularly for multi-year events, necessitating the exploration of novel insights and potential precursors.

The North Pacific Eastern Subtropical Mode Water (NPESTMW) presents an intriguing candidate for investigation in this context. NPESTMW is a distinct water mass formed in the northeastern Pacific (Fig. S1a), the origin region of PMM. The PMM can induce significant atmospheric changes in this region, including anomalies in wind stress and surface heat flux[20], which are critical drivers of mode water formation through subduction process [24,25]. Moreover, as an integral part of the subtropical cell (STC) —a shallow meridional overturning circulation consisting of subtropical subduction, equatorward advection of cool subsurface water, upwelling at the equator, and poleward return of surface warm water[26]—NPESTMW plays an important role in transporting heat, salt, and tracers from the subtropics to the tropics. This circulation bridges subtropical and tropical domains, influencing tropical climate variability[27–29]. Given its unique geographical positioning and its connection to the STC, NPESTMW offers a promising yet unexplored connection between subtropical processes and tropical Pacific climate variability.

Here we employ multiple data sources, including observational data, reanalysis products, and numerical model results, to investigate the potential relationship between NPESTMW and ENSO occurrence and evolution, and elucidate the physical mechanism linking NPESTMW to tropical Pacific variability. By exploring these connections, we aim to bridge the gap between subtropical oceanic processes and tropical climate phenomenon,

[1]Key Laboratory of Ocean Observation and Forecasting and Key Laboratory of Ocean Circulation and Waves, Institute of Oceanology, Chinese Academy of Sciences, Qingdao, China. [2]Department of Earth System Science, University of California, Irvine, CA, USA. [3]Laboratory for Ocean Dynamics and Climate, Qingdao Marine Science and Technology Center, Qingdao, China. [4]Research Center for Critical Issues, Academia Sinica, Taipei, Taiwan. ✉e-mail: liull@qdio.ac.cn; jyyu@uci.edu

potentially revealing new factors associated with ENSO evolution and persistence.

Results

Connecting NPESTMW volume anomalies to ENSO

The formation and properties of NPESTMW, including thickness, temperature, and density, exhibit significant interannual variations[24,30]. Analysis of the ensemble mean (EM) results, which represent the average from IAP, EN4, GODAS, and SODA3.4.2, reveals a statistically significant correlation between NPESTMW volume anomalies and the November-December-January Ocean Niño Index (ONI) (Fig. 1). This correlation reaches its negative peak at a 9-month lag ($r = -0.69$, $p < 0.01$), with ONI lagging behind NPESTMW, and persists for lag times up to 16 months. The 9-month lag indicates that ENSO events, which typically peak in December, are highly correlated with the NPESTMW volume measured in the preceding March. Despite discrepancies in detail, the robust negative correlation between March NPESTMW volume anomaly and ONI is consistently reproduced by all four individual datasets (Fig. S2). These findings suggest that March NPESTMW volume anomalies may contribute to the predictability of ENSO events. Since ENSO can influence subtropical North Pacific atmospheric processes[31,32], it is important to examine whether the relationship between NPESTMW and subsequent ENSO development simply reflects ENSO's autocorrelation, as suggested by previous studies[33,34]. If NPESTMW variability were merely a reflection of autocorrelation, we would expect significant correlations when ENSO leads NPESTMW. However, no such significant correlation exists (Fig. 1). We further examined the ENSO conditions in the year preceding the large NPESTMW volume anomaly. Between 1991 and 2022, we identified nine positive NPESTMW anomaly events and eight negative events, with the EM March NPESTMW volume anomalies exceeding ±0.6 standard deviations, respectively. The result reveals that among the nine positive NPESTMW anomaly events, four were preceded by El Niño and four by La Niña conditions. Of eight negative NPESTMW anomaly events, only one followed La Niña and one followed El Niño conditions (Table S1). This inconsistent relationship with preceding-year ENSO states suggests that NPESTMW variations are not merely a passive response to ENSO. Rather, the lead-lag relationship between NPESTMW with subsequent ENSO events likely involves complex mechanisms beyond ENSO's autocorrelation. Supporting this conclusion, our analysis shows that following large positive NPESTMW anomaly events, eight La Niña events and one neutral (non-ENSO) event occurred, while following negative NPESTMW anomaly events, seven El Niño events and one neutral event were observed (Table S1).

The annual cycle of NPESTMW volume indicates that March NPESTMW predominantly forms during the preceding winter months (Fig. S1b). Previous studies have demonstrated that mixed layer depth variations significantly influence NPESTMW formation through subduction process [35–37]. The PMM, a prominent pattern of climate variability in the subtropical northeastern Pacific, exerts substantial influence on regional ocean-atmosphere interactions. Our analysis reveals a robust negative correlation between the EM March NPESTMW volume anomalies and the preceding wintertime (January-February-March) PMM wind index ($r = -0.49$, $p < 0.01$; Fig. 2a), reflecting PMM's important role in NPESTMW formation region (Fig. 2b). This relationship is consistently captured across all four datasets, with GODAS and SODA3.4.2 exhibiting the correlation in May (Fig. S3). Moreover, the consistency of these findings when using the alternative PMM SST index (Fig. S4) further validates the significant impact of PMM in the NPESTMW formation area. Positive PMM events are marked by unusual southwesterly winds and warmer-than-average SSTs in the subtropical northeastern Pacific. These conditions hinder the formation of NPESTMW by reducing wind stress amplitude (Fig. 2c), decreasing net surface heat loss (Fig. 2d), and enhancing freshwater gain (Fig. 2e). These factors collectively contribute to a diminished air-sea buoyancy flux and weakened diapycnal mixing, resulting in a shallower mixed layer and inhibited mode water formation. Conversely, negative PMM phases exhibit opposite tendencies, fostering conditions conducive to enhanced NPESTMW formation. This mechanism is further substantiated by subduction rate calculation, which consistently shows smaller subduction rates during positive PMM events compared to negative phases in the NPESTMW formation region (Fig. S5).

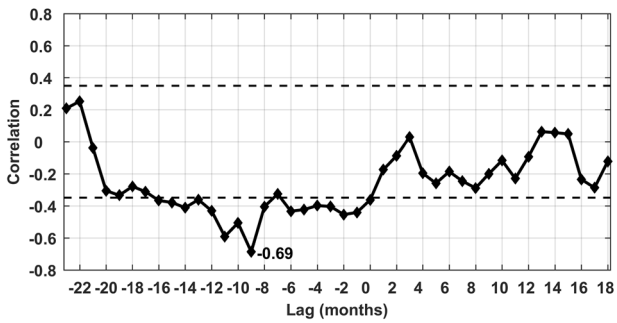

Fig. 1 | Correlations between NPESTMW and ENSO. Lead-lag correlations between the ensemble mean (EM) NPESTMW volume anomalies and the November-December-January ONI for the period 1991–2022. Dashed lines represent the 95% confidence level. Positive lags denote ONI leading NPESTMW volume anomalies. The EM represents the average of NPESTMW volume anomalies from IAP, EN4, GODAS, and SODA3.4.2.

To elucidate the relationship between NPESTMW volume variability, PMM, and potential ENSO development, we analyze SST evolution during PMM-related NPESTMW volume anomaly events. Among nine positive NPESTMW anomaly events, seven are linked to negative PMM events, while four of the eight negative NPESTMW anomalies coincide with positive PMM events, defined by January-February-March PMM indices surpassing ±0.5 standard deviations (Table S1). As shown in Fig. 3a–j, the SST anomalies in the tropical central Pacific appear as early as March (during NPESTMW formation) and develop into ENSO-like SST patterns in subsequent months. The positive NPESTMW volume anomaly event, linked to negative PMM phases, often leading to La Niña events. Conversely, negative NPESTMW volume anomaly events, associated with positive PMM phases, often leading to El Niño events. It is noted that this pattern remains robust regardless of the threshold chosen for defining NPESTMW anomaly strength (figure omitted). Further analysis reveals that these PMM-related NPESTMW anomaly events are particularly associated with Central Pacific (CP) ENSO events. Specifically, among the seven positive PMM-related NPESTMW anomaly events, six were followed by La Niña, with four being CP-type La Niña. Similarly, for the four negative PMM-related events, three were followed by El Niño, two of which were being CP-type (Table S1). These findings align with the subtropical ENSO dynamics mechanism, where positive (negative) PMM can initiate CP El Niño (La Niña) events through wind-evaporation-SST (WES) feedback[22,38].

These findings suggest that anomalous NPESTMW volume events can serve as indicators of forthcoming ENSO events, reflecting PMM activity. As NPESTMW volume variations are linked to PMM through PMM-related atmospheric forcing on the ocean, a remote driver known to excite PMM can therefore influence NPESTMW volume variations through similar mechanisms. For instance, the SST anomalies in the tropical North Atlantic (TNA), an important source of external forcing to excite the PMM[39], show a significant correlation ($r = 0.37$, $p < 0.05$) with EM March NPESTMW volume anomalies. Warm TNA SSTs can induce a Gill-type cyclonic circulation in the eastern Pacific that strengthens northeasterly winds, simultaneously triggering negative PMM through WES feedback and enhancing NPESTMW formation through increased wind stress and heat loss. This suggests that PMM and NPESTMW variations could be responding to the same forcing field through related changes in wind stress and heat flux. While variations in NPESTMW volume do not directly influence ENSO events in this mechanism, they offer distinct, complementary information to PMM and may be valuable as early oceanic indicators for ENSO evolution.

In non-PMM years (Fig. 3k–t), the SST patterns during positive and negative NPESTMW anomaly events show prominent equatorial Pacific

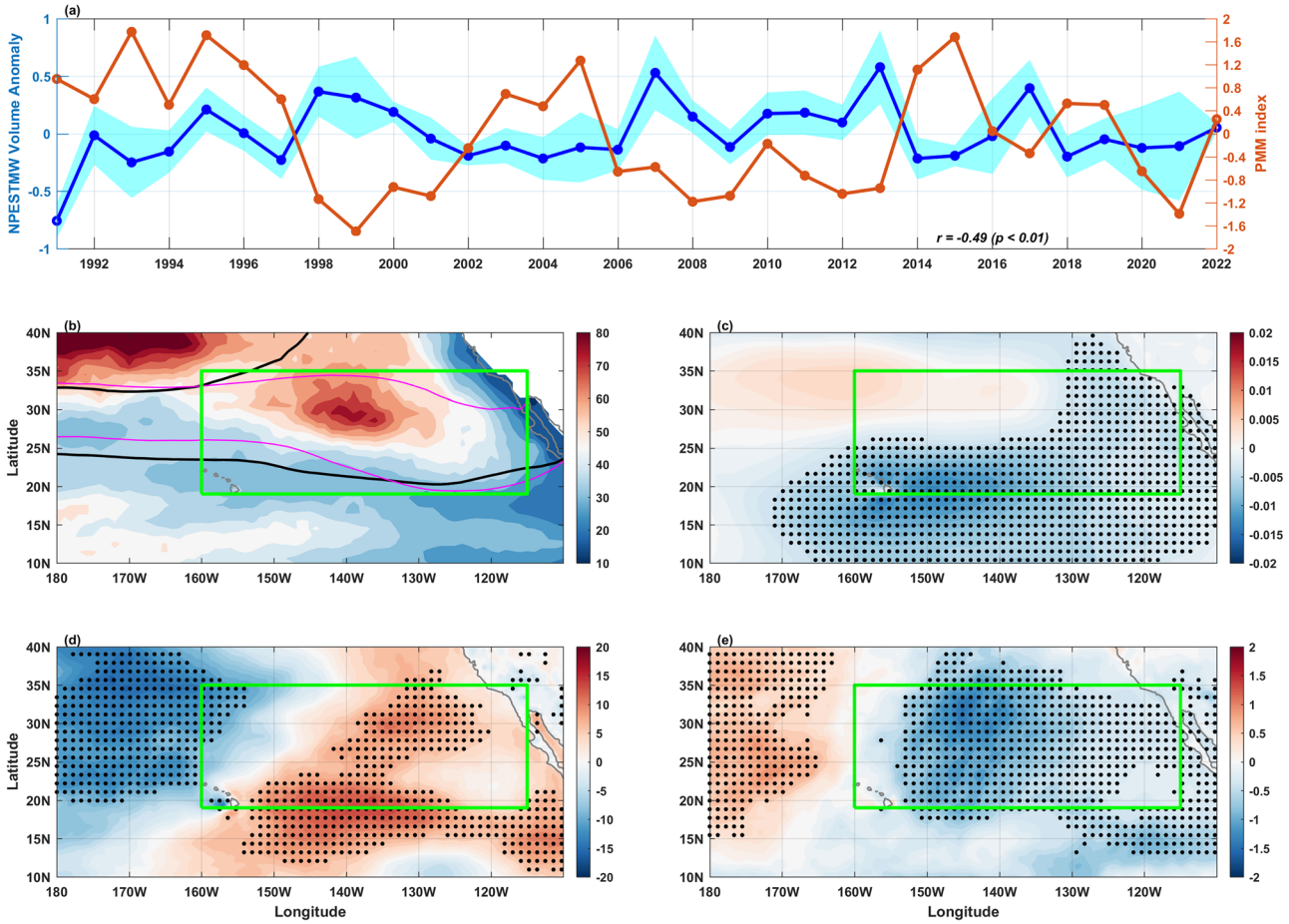

Fig. 2 | Relationship between March NPESTMW volume anomalies, PMM, and associated atmospheric forcings. a Timeseries of ensemble mean (EM) March NPESTMW volume anomalies (blue) and normalized January-February-March PMM wind index (orange), with correlation coefficient indicated. **b** EM late-winter sea surface conditions: mixed layer depth (colors), sea surface potential density (black contours; 24 and 25.4 kg m^{-3}), and sea surface temperature (pink contours; 16 and 22 °C). The EM represents the average from IAP, EN4, GODAS, and SODA3.4.2. **c**–**e** Regression of normalized PMM index against **c** wind stress amplitude, **d** net downward surface heat flux, and **e** evaporation minus precipitation, averaged in January-February-March. Stipplings denote regions significant at a 95% confidence level (Student's *t*-test). Green boxes denote the NPESTMW formation region.

anomalies, though with distinct features compared to PMM-related events. It is seen that positive NPESTMW anomalies can lead to cold SST anomalies in the equatorial Pacific from July onward, potentially favoring La Niña development, while negative NPESTMW anomalies may promote El Niño development. This result indicates that March NPESTMW volume variations could be connected to ENSO events even without PMM influence. While ENSO can influence subtropical North Pacific atmospheric processes, suggesting a possible autocorrelation effect[33,34], our analysis reveals a more complex picture. From Fig. 3k–o, warm signals in the tropical Pacific are evident in March, and Tabel S1 statistics confirm that both positive non-PMM–NPESTMW anomaly events were preceded by El Niño events in the previous year. However, among negative non-PMM anomaly events, only one was preceded by La Niña, partially supporting the ENSO autocorrelation hypothesis. Importantly, three events were preceded by neutral conditions, suggesting the existence of an alternative mechanism through which NPESTMW may influence ENSO development, which were distinct from PMM influence and ENSO autocorrelation.

Using Lagrangian particle tracking analysis which are widely used to trace the sources/destinations of subsurface water-mass[40,41], there are two distinct pathways through which the STC transports water from eastern subtropical Pacific to the equatorial Pacific (Fig. 4a). The first is the western-boundary route, where water parcels are transported westward the Pacific western boundary before reflecting toward the equator. The second is the interior route, characterized by southward penetration followed by a southeastward turn. The western-boundary route has a longer transit time of 5–10 years[29], through which the spiciness anomaly can be advected from the eastern subtropical Pacific to the tropical western Pacific, with some portion overshooting toward the eastern equatorial Pacific[42]. This overshooting aligns with Fukumori et al[43], who demonstrated that intra-annual variability of the velocity field enhances tracer transports from the subtropics to the equator through an interior path. Water parcels following the interior pathway reach the tropical ocean more rapidly, typically within 3–4 years based on the climatological mean velocity fields (Fig. 4a), and this timescale is substantially shortened during the positive NPESTMW anomaly events as demonstrated in the subsequent analysis. Since this study specifically investigates the connection between NPESTMW volume anomalies and ENSO at timescales shorter than 5–10 years, we focus primarily on the faster interior pathway rather than the western-boundary pathway.

As shown in Fig. 4a, the interior pathway associated with NPESTMW is mainly located within 170°E and 148°W at 9°N. This latitude (9°N) represents a choke point for meridional geostrophic transports in the interior ocean[29]. This pattern demonstrates NPESTMW as a component of the STC branch through the interior pathway, with its formation via subduction reflecting changes in this STC branch. Further analysis indicates that March NPESTMW volume exhibits a significant negative correlation with meridional current anomalies crossing 9°N, which is calculated as the averaged anomaly between 170°E and 148°W within the density range of

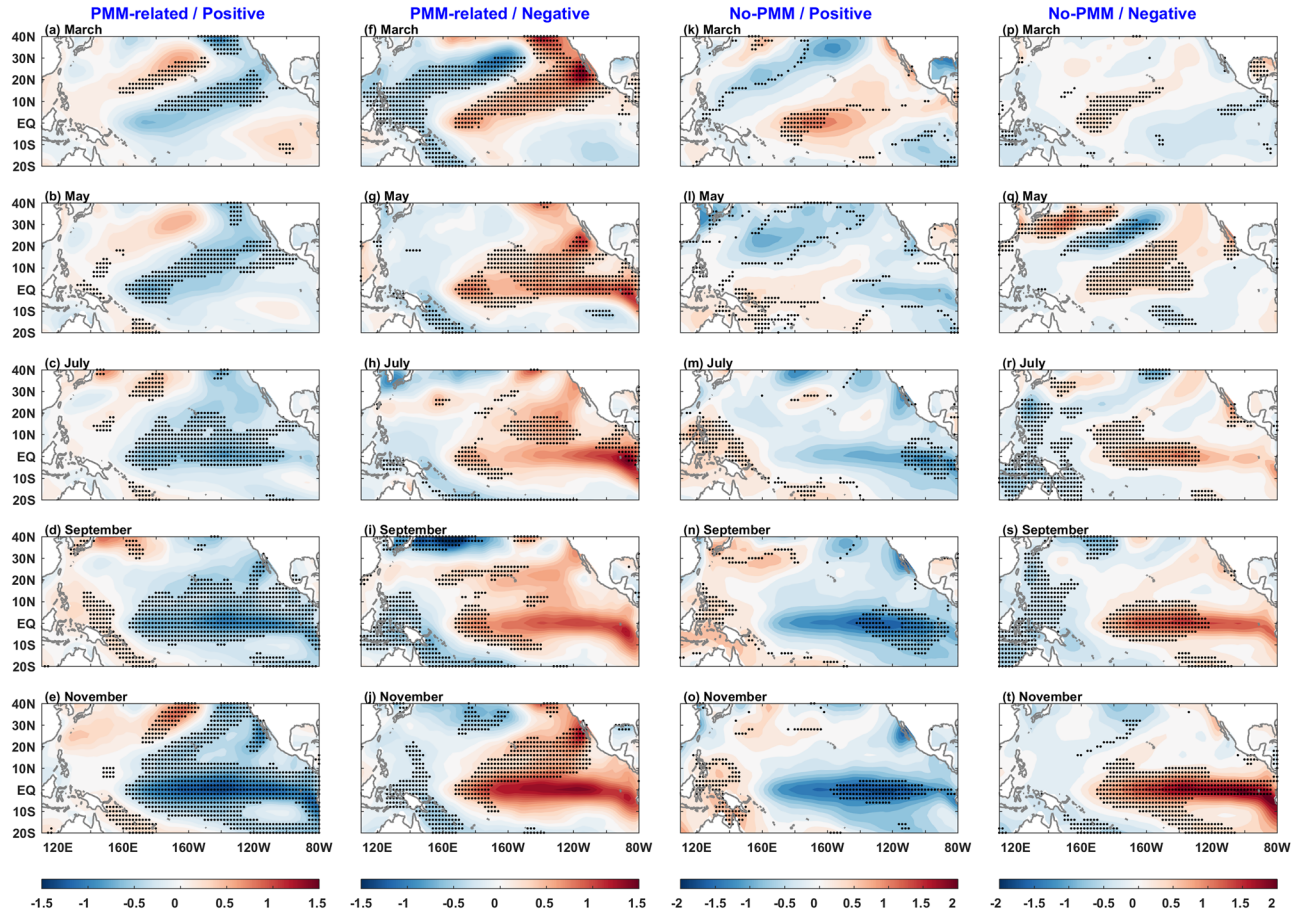

Fig. 3 | Sea surface temperature (SST) evolution associated with NPESTMW volume anomalies. Observed SST anomaly during years with PMM-related (**a**–**j**) and no-PMM (**k**–**t**) positive (**a**–**e**, **k**–**o**) and negative (**f**–**j**, **p**–**t**) NPESTMW volume anomalies. NPESTMW anomaly years are defined by ensemble mean March NPESTMW volume anomalies exceeding ±0.6 standard deviations. PMM-related events are identified when the January-February-March PMM index exceeds ±0.5 standard deviations. Stipplings denote region significant at 90% confidence level (Student's *t*-test).

24.2–25.4 kg m^{-3} (the typically density range of NPESTMW; Fig. S6), and this significant correlation persists from three months later until March of the following year (i.e., 12-month lag) (Fig. 4b). From July onwards, the meridional current anomaly crossing 9°N displays a significant positive correlation with the November-December-January ONI (Fig. 4c). These findings suggest that a positive NPESTMW volume anomaly in March, triggered by unusually strong subduction, can enhance the southward transport of cooler water toward the equatorial central Pacific, thereby promoting La Niña development. Conversely, a negative NPESTMW volume anomaly can support El Niño development through a similar oceanic pathway. Although there are some differences in the details, both GODAS and SODA3.4.2 reanalysis datasets confirm the significant relationships between meridional current anomalies crossing 9°N, NPESTMW volume, and tropical Pacific SST (Fig. S7). It is consistent with previous studies that an increase/decrease in STC equatorward mass transport enhances/weakens equatorial upwelling, bringing more/less cold pycnocline waters closer to the surface and cooling/warming SSTs[29,44,45]. This process encapsulates the recharge-discharge of the equatorial upper ocean heat content at interannual timescales, underpinning ENSO evolution[46].

Our results reveal a sequential connection between NPESTMW formation, STC interior transport toward the equator, and subsequent ENSO development. This highlights a distinct pathway linking NPESTMW anomaly to tropical Pacific climate variability via the STC mechanism, operating independently from both PMM and preceding ENSO events influence. Importantly, NPESTMW impacts tropical Pacific SST not through the physical arrival of mode water itself, but as an indicator of STC interior pathway transport intensity, affecting tropical Pacific SST development through circulation changes. We acknowledge that the limited sample size introduces statistical uncertainties. While ENSO development involves multiple concurrent precursor signals, the extent of NPESTMW's independent influence on ENSO beyond established precursors remains an open question. Further studies with extended datasets and specially designed model experiments are needed to quantitatively isolate these effects.

Enhanced NPESTMW volume anomalies linked to multi-year ENSO events

While ENSO events typically last for ~1 year, some persist into subsequent years, becoming multi-year (MY) events. MY La Niña events, in particular, have been associated with distinct or even more severe climate impacts compared to single-year (SY) events[47–51]. The CESM preindustrial simulation captures the general spatial and temporal characteristics of NPESTMW, albeit with a more southward distribution (Fig. S1). The CESM simulation effectively reproduces the correlation between NPESTMW and ENSO (Fig. S8). Compared to observations where NPESTMW volume anomalies show the strongest correlation with ONI in March, CESM simulates the strongest correlation in May. This 2-month lag may be attributed to the model bias in representing ocean stratification or winter mixing processes that could affect the timing of NPESTMW formation. Additionally, the relatively coarse resolution may impact the simulation of atmospheric forcing fields and air-sea interaction processes, and thus the NPESTMW. Furthermore, given that PMM is a key driver of NPESTMW formation, biases in the timing or amplitude of PMM variability in CESM may also contribute to this lag, as delayed or altered PMM development

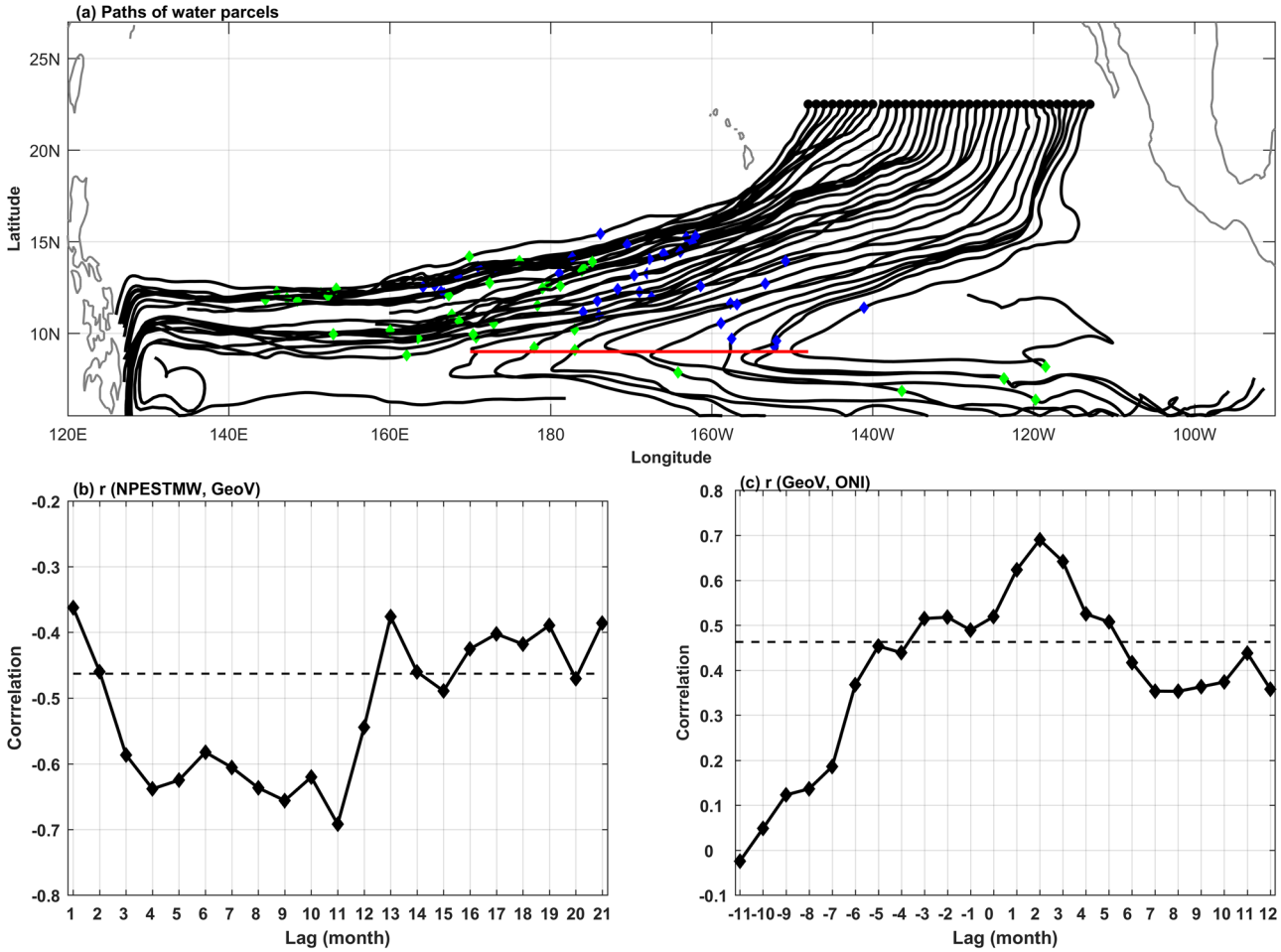

Fig. 4 | Subtropical-tropical water exchange and its relationship with NPESTMW and ENSO. a Lagrangian trajectories initiated at 22.5°N at 60 m depth, calculated using IAP and NCEP/NCAR wind stress. Blue and Green diamonds represent the location of trajectories after tracing 3 and 4 years. The red line indicates the subtropical-tropical water exchange window (interior pathway) at 9°N. **b** Cross-correlation between March NPESTMW volume anomalies and meridional current anomalies, as a function of NPESTMW lead time. **c** Cross-correlation between meridional current anomalies and November-December-January ONI. Negative lags indicate meridional current anomalies leading to ONI. Dashed lines in **b**, **c** represent the 99% confidence levels. Meridional current anomaly is defined as the averaged anomaly between 170°E and 148°W (red line in a) at 9°N within the density range of 24.2–25.4 kg m^{-3}.

would directly influence the timing of NPESTMW formation. Nevertheless, it is worth noting that CESM still captures a significant correlation between March NPESTMW volume and ONI. In the following CESM analysis, we use the May NPESTMW volume and the preceding March-April-May PMM index, when PMM reaches the peak (figure omitted), as key indicators, finding a correlation coefficient of −0.77 ($p < 0.01$) between them. It is noted that the PMM–NPESTMW relationship is not sensitive to the specific choice of months used to define the PMM events: r between NPESTMW volume anomalies and PMM averaged over January-March (−0.76) and February-April (−0.77) are comparable to those using March-May average. This robustness can be attributed to the strong temporal coherence of the monthly PMM index from January to May, with r all exceeding 0.63 (significant at 99% confidence level). The model reasonably replicates the observed PMM-related atmospheric forcing conditions over the NPESTMW formation region (see Fig. S9 and Fig. 2). Additionally, the CESM simulation accurately reproduces the development of a La Niña event following a PMM-related positive NPESTMW volume anomaly (Fig. S10a–e) and an El Niño event following a PMM-related negative NPESTMW volume anomaly (Fig. S10f–j).

It is important to note that in the CESM simulation, all water masses in the NPESTMW region enter the equatorial Pacific via the western boundary (Fig. S11), indicating that CESM does not capture the STC branch through the interior pathway. As a result, no ENSO-like SST pattern develops in the tropical Pacific during the subsequent winter for non-PMM–NPESTMW anomaly events in the model (Fig. S10k–t). This missing STC interior pathway in CESM may be linked to the coarse model resolution, the parameterization of vertical mixing processes, or the surface forcing bias in the coupled model, warranting detailed analysis in the future. Despite this limitation, CESM effectively represents the relationships among NPESTMW, PMM, and ENSO, making it a valuable tool for studying these complex climate interactions.

Both observations and the CESM simulation reveal enhanced NPESTMW thickness anomalies preceding MY ENSO events compared to SY events, with this difference being more pronounced for the La Niña phase (Fig. 5a–d and Fig. S12). We further analyze the frequency distribution of SY and MY ENSO events as a function of May NPESTMW volume anomaly threshold in the CESM simulation (Fig. 5e). The results demonstrate a clear trend: as NPESTMW anomalies intensify, the proportion of MY events increases significantly, particularly for La Niña events. When NPESTMW volume anomalies exceed 0.1×10^{14} m^3 and a La Niña event occurs, 62% of these events persist for multiple years. This proportion rises dramatically with increasing NPESTMW volume anomaly magnitude: 76% of La Niña events are MY when NPESTMW anomalies surpass 0.7×10^{14} m^3, reaching 100% for anomalies exceeding 0.9×10^{14} m^3. While a similar trend is observed for El Niño events, the effect is less pronounced. The proportion of MY El Niño events increases from 39% when negative

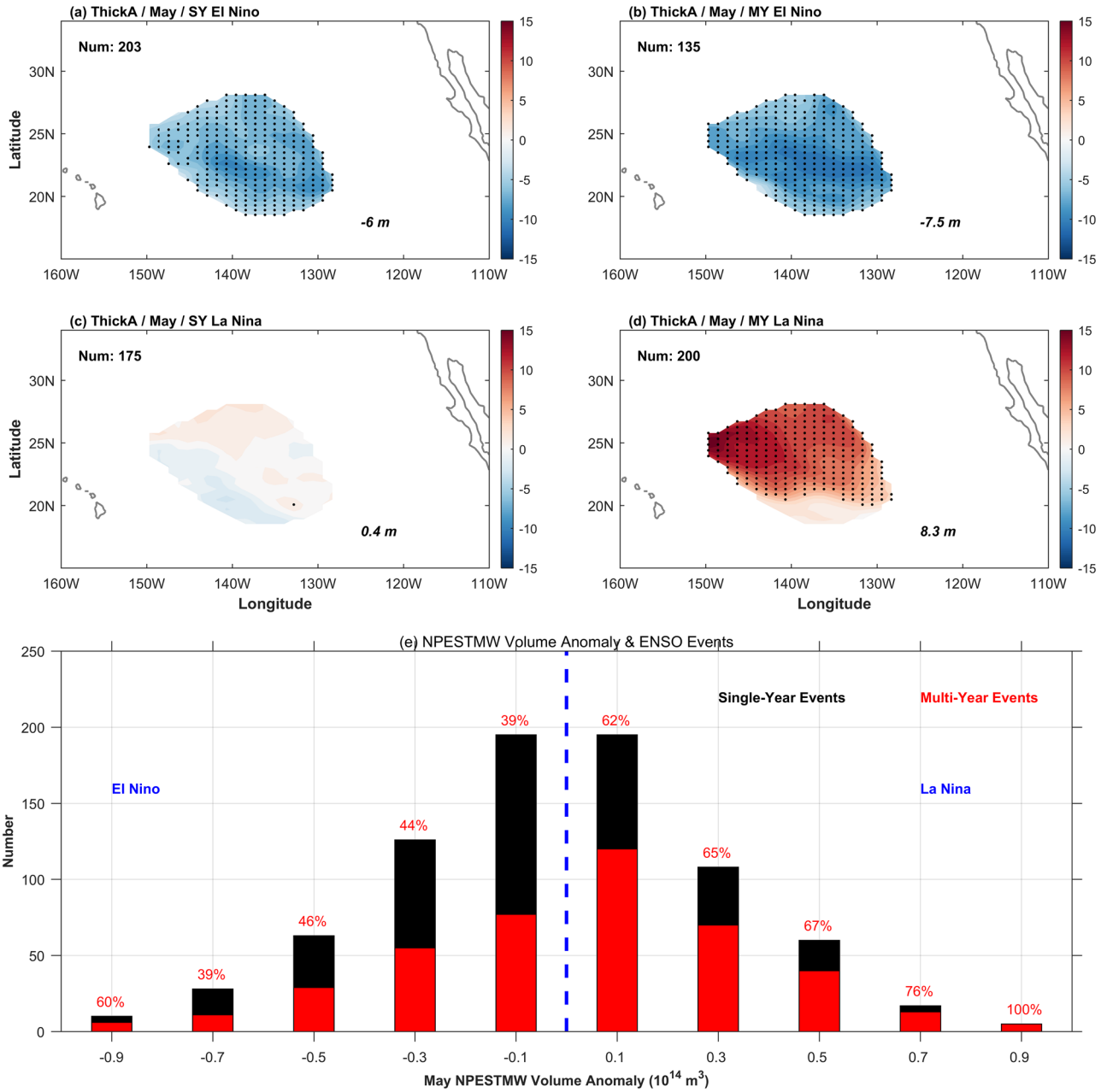

Fig. 5 | NPESTMW anomalies and ENSO event classification in CESM simulation. a–d Composite May NPESTMW thickness anomalies during single-year (**a**, **c**) and multi-year (**b**, **d**) El Nino (**a**, **b**) /La Nina (**c**, **d**) events, respectively. Insets: event frequency and region-averaged thickness anomalies. Stipplings indicate regions that are statistically significant at the 95% confidence level based on Student's *t*-test. **e** Frequency distribution of single-year (black) and multi-year (red) ENSO events as a function of May NPESTMW volume anomaly threshold, with multi-year event proportion expressed as a percentage.

NPESTMW anomalies exceed 0.1 × 10^{14} m^3 to 60% when anomalies surpass 0.9 × 10^{14} m^3.

As discussed above, NPESTMW, as a subtropical footprint of PMM, reflects the PMM's role in triggering ENSO. Previous studies have identified the crucial role of the PMM mechanism in driving the MY ENSO events. The PMM's northeast-southwest orientation generates CP SST anomalies[22,52], and the resulting CP ENSO can subsequently activate another PMM via atmospheric wave trains, leading to another ENSO with the same phase and resulting in a MY event[32,53–56]. In other words, there will be another same-phase anomaly in the equatorial Pacific corresponding to the PMM event triggered by ENSO in the second year. Moreover, the asymmetry corroborates previous findings that the cold phase of PMM demonstrates higher efficacy in inducing subsequent La Niña events compared to the warm PMM's ability to induce El Niño events[57].

Moreover, it is well-documented that MY La Niña events frequently follow strong El Niño, which characteristically induce significant negative PMM signals during the subsequent spring[58]. Therefore, some MY La Niña signals in Fig. 5e may actually represent an indirect consequence of preceding strong El Niño events. To verify this possibility, we arbitrarily selected samples in Fig. 5e that have NPESTMW volume anomalies between 0.5 and 0.7 × 10^{14} m^3. Among the 27 MY La Niña events that followed these samples, 11 events were preceded by an El Niño year. Furthermore, in eight of these cases, the averaged ONI during the preceding November-January period exceeded 1 °C, indicating a strong El Niño event. Different NPESTMW anomaly thresholds would give rise to a similar pattern. In general, among the MY La Niña events that followed the NPESTMW volume anomalies exceeded 0.1 × 10^{14} m^3, ~35% were preceded by a strong El Niño event. This sequential pattern suggests that for a substantial portion

of events, the relationship between NPESTMW and MY La Niña events may be influenced by the preceding El Niño forcing.

A third factor to consider is the NPESTMW-related STC branch. Based on our comparative analysis of the STC branch during years with strong positive versus negative NPESTMW anomalies, both observation and reanalysis datasets consistently reveal enhanced transport through the STC interior pathway during the positive NPESTMW anomaly events (Fig. S13). Furthermore, IAP (pure observational data) shows an accelerated transport from the subtropics to the tropics under positive NPESTMW conditions, with the transport timescale reduced to 2–3 years (Fig. S13a), while under negative anomaly conditions, the transport is 3–4 years (Fig. S13b). Overall, on average, there exists an anomalous equatorward mass transport through the STC interior pathways within 2 years following a NPESTMW anomaly. Indeed, as shown in Fig. 4b, the significant correlation between March NPESTMW anomalies and subtropical-tropical exchange through the interior pathway exists up to 15 months later, which in turn relates to tropical Pacific SST during the ENSO development phase (June-July-August season, Fig. 4c). GODAS and SODA3.4.2 yield similar conclusions, with differences in the correlation persistence timeframe (Fig. S7).

Similar conclusions can be drawn regarding the equatorial upwelling, the ascending branch of the STC. To ensure a balanced distribution across different event categories, we separate NPESTMW anomaly years into strong and weak groups based on the criteria of 0.8 standard deviations. Under weak NPESTMW volume anomaly conditions, equatorial upwelling anomalies reveal varying responses across datasets. Observation datasets (using sea level anomaly as a proxy for vertical velocity) show SLA sign reversal from year 0 to year 1 (Fig. S14c, d, g, h), while reanalysis datasets exhibit upwelling anomaly patterns opposite to strong NPESTMW anomaly events (Figs. S15, S16). Despite these discrepancies in weak anomaly cases, all data sources demonstrate consistent equatorial upwelling anomalies during strong NPESTMW anomaly events, though with some differences in detail. Strong positive (negative) NPESTMW anomalies are associated with enhanced (weakened) equatorial Pacific upwelling, which persists into the second year (year 1) with same-phase upwelling anomalies (panels a, b, e, f in Figs. S14–16). This persistence facilitates the continuation of ENSO events over multiple years. Notably, this pattern remains robust regardless of the threshold chosen for defining NPESTMW anomaly strength (figure omitted).

Discussion

This study provides novel insights into the relationship between subtropical ocean processes and ENSO dynamics, revealing significant correlations between NPESTMW volume anomalies and ONI up to 16 months in advance. Our analysis identifies two distinct pathways through which NPESTMW is associated with ENSO events: the PMM-related mechanism and the subtropical-tropical exchange through the interior ocean window. A key finding is asymmetry in NPESTMW's association with MY ENSO events, particularly its strong correlation with La Niña. These discoveries contribute to our understanding of long-term climate variability, particularly regarding the onset and duration of MY La Niña episodes.

NPESTMW volume anomaly is intricately connected to other established ENSO precursors. As a footprint of PMM events in the subtropical Pacific, NPESTMW volume anomaly effectively represents PMM variations, which can further regulate subsurface heat content in the equatorial Pacific through trade wind charging mechanisms[59]. Therefore, NPESTMW volume anomaly can, to some extent, reflect PMM's role as a precursor to ENSO events. Moreover, NPESTMW volume anomaly can influence the equatorial Pacific Warm Water Volume (WWV) through mass transport via the STC interior pathways. While WWV and western Pacific Warm Water Volume (WWV_w) are well-established and reliable indicator of ENSO evolution[60,61], NPESTMW may offer additional predictive value by providing early signals of ENSO development from the subtropical ocean, particularly for MY events.

Future studies could focus on further validating NPESTMW volume as a reliable early warning indicator for ENSO events, especially for MY events. We need to further explore the underlying causes of the asymmetry in the relationship between NPESTMW volume and El Niño versus La Niña events and examine its role in specific ENSO events that are not fully captured by WWV or WWV_w alone. However, our study also reveals important limitations in model simulations. The failure of CESM to reproduce the STC branch through the interior pathway underscores the complexity of the mechanisms involved and highlights critical areas for model improvement. To incorporate NPESTMW into current prediction systems, climate models must first accurately simulate the formation and evolution of NPESTMW, associated with the better representation of subtropical-tropical interaction and the STC. Building on this foundation, the ENSO development phase prediction skill could be potentially improved by incorporating NPESTMW volume anomalies as initial conditions in climate models and quantitatively evaluating their contribution to forecast skill improvement. Additionally, understanding how NPESTMW characteristics might change under different climate scenarios could help enhance the reliability of long-term ENSO projections. Such integration of NPESTMW into the prediction framework could significantly advance our ability to forecast ENSO events with greater accuracy and longer lead times.

Methods

Observational data and climate indices

To characterize mode water properties, we employ four distinct datasets: two observational products (IAP and EN4) and two reanalysis datasets (SODA3.4.2 and GODAS). The Institute of Atmospheric Physics (IAP) dataset[62] provides monthly temperature, salinity, and geostrophic currents data on a 1° × 1° grid with 41 vertical layers to 2000 m depth. The EN4 dataset (v4.2.2-analyses-g10) from Met Office Hadley Centre[63] offers monthly temperature and salinity data across 42 depth layers. These observational products are derived from quality-controlled in situ measurements and are subjected to objective analysis procedures. In contrast, the simple ocean data assimilation (SODA) version 3.4.2[64] is based on the Geophysical Fluid Dynamics Laboratory (GFDL) Modular Ocean Model (MOM) version 5 ocean model with 0.25° × 0.25° horizontal resolution and 50 vertical layers, forced by ERA-interim near-surface atmospheric variables, and employs the SODA3 assimilation system that incorporates various in situ and satellite observations. The National Center for Environmental Prediction (NCEP) Global Ocean Data Assimilation System (GODAS)[65] utilizes the GFDL MOM3 ocean model with 1° × 1° horizontal resolution (enhanced to 1/3° in the tropics) and 40 vertical layers, with atmospheric forcings from NCEP atmospheric Reanalysis 2, and assimilates temperature profiles using a 3D-VAR scheme. Here, we use the ensemble mean of all four datasets to enhance the robustness of our findings. The study period spans 1991–2022, coinciding with the earliest transects across the northeast Pacific[66].

The Extended Reconstructed Sea Surface Temperature (ERSST) version 5 provided by the National Centers for Environmental Information/National Oceanic and Atmospheric Administration are used to depict the SST evolution[67]. Surface heat fluxes, wind vectors, evaporation and precipitation are from the Japanese 55-year reanalysis (JRA-55)[68]. The monthly PMM wind and SST index and TNA index are provided by the National Oceanic and Atmospheric Administration (NOAA) Earth System Research Laboratory (ESRL). The ENSO index, including ONI, Niño1 + 2 index, and Niño4 index, are obtained from the NCAR climate-data guide.

CESM1 and climate indices

To enhance our analysis beyond the limited ENSO events in observational data, we utilize model years 400-2200 of the 2200-year CESM1 preIndustrial Control Simulation[69]. This model has demonstrated capability in reproducing observed ENSO characteristics and the contrasting features of SY and MY ENSO events[50,55,70–73]. We define the ONI as 3-month running mean SST anomalies averaged over 5°S–5°N, 170°–120°W. The PMM index is calculated as the SST anomalies averaged in the subtropical northeastern Pacific (10–30°N, 115–155°W)[74,75].

Identifying ENSO events

An El Niño or La Niña event is identified if the ONI exceeds ± 0.5 °C during November to January. The onset year is designated as year 0, with subsequent years labeled as year 1, year 2, etc., for all calendar months. For the CESM1 simulation, we recognize events when the first winter ONI (November^0– January^1) exceeds ± 0.5 standard deviations (0.57 °C).

We classified ENSO events as single-year (SY) or multi-year (MY) events based on the second winter's ONI. For El Niño, an ONI ≤ 0.3 °C defines a SY event, while ONI >0.3 °C indicates a MY event. Conversely, for La Niña, an ONI ≥ −0.3 °C in the second winter characterizes a SY event, while ONI <−0.3 °C denotes a MY event. For CESM1, the SY or MY events was similarly defined based on the second winter's ONI with the thresholds of ± 0.3 standard deviations (0.34 °C). We further tested the sensitivity of our results by using alternative thresholds, e.g., 0 °C used in previous studies[19,50,51,76], to classify SY and MY events. Similar conclusions are obtained, indicating that our findings are robust regardless of the specific ONI cutoff chosen. We determine ENSO events as EP (CP) type if the absolute value of their winter Niño1 + 2 index is greater (less) than the Niño 4 index.

Mode water definition and subduction rate

Mode water is characterized by a vertically uniform water mass layer. For NPESTMW specifically, previous studies[66,77–79] have identified it as a low-potential vorticity (PV) water ($2-5\times10^{-10}\,m^{-1}\,s^{-1}$). We calculate PV as $PV=-(f/\rho_0)\partial\sigma_\theta/\partial z$, where $\rho_0=1025\,kg\,m^{-3}$ is the reference density, f is the Coriolis parameter, σ_θ is the potential density, and z is the vertical coordinate (positive upward). We neglect relative vorticity in this calculation. Observations show that the low-PV water mass in the subtropical eastern North Pacific is primarily confined within the density range of 24.0–25.5 kg m^{-3} (Fig. S4), which is consistent with previous studies[80]. Here we identify NPESTMW as low-PV water (PV $<3.0\times10^{-10}\,m^{-1}\,s^{-1}$) with σ_θ between 24.0 and 25.5 kg m^{-3} beneath the surface mixed layer. The mixed layer depth is calculated as the depth where the potential density is larger than that at 10-m depth by 0.03 kg m^{-3} [81]. We also computed the mixed layer depth with other density criteria such as 0.125 kg m^{-3}, and it was found that the conclusions are insensitive to the choice of density criterion.

The annual subduction rate is calculated in Lagrangian coordinates using the following formula[40]:

$$S_{ann}=-\overline{\left(W_{ek}-\frac{\beta}{f}\int_{-h_m}^{0}v\,dz\right)}+\frac{1}{T}\left(h_{m,0}-h_{m,1}\right). \quad (1)$$

Here, $W_{ek}=\frac{1}{\rho}curl\left(\frac{\tau}{f}\right)$ is the Ekman pumping velocity. τ is the surface wind stress, and ρ is the seawater density. β is the meridional derivative of the Coriolis parameter f, v is the meridional velocity. The overbar represents the averaged along 1-year Lagrangian trajectory, $T=1$ year; $h_{m,0}$ and $h_{m,1}$ represent the mixed layer depth at the beginning and ending locations of the 1-year Lagrangian trajectory.

Data availability

All data used in this study are publicly available. IAP data were available from http://www.ocean.iap.ac.cn/pages/dataService/dataService.html. EN4 data were available from https://www.metoffice.gov.uk/hadobs/en4/. SODA3.4.2 data were available from https://www2.atmos.umd.edu/~ocean/; GODAS data were available from https://www.cpc.ncep.noaa.gov/products/GODAS/; JRA55 data are from http://rda.ucar.edu/datasets/ds628.1/; ERSST data were available from https://www.ncei.noaa.gov/products/extended-reconstructed-sst. The CESM simulation outputs are available from https://www.cesm.ucar.edu/community-projects/lens/data-sets. The PMM index is available from https://psl.noaa.gov/data/timeseries/monthly/PMM/. The TNA index is available from https://psl.noaa.gov/data/timeseries/month/DS/TNA/.The ENSO index is available from https://climatedataguide.ucar.edu/climate-data/nino-sst-indices-nino-12-3-34-4-oni-and-tni.

Code availability

The codes used to replicate all the results in this study can be obtained from the authors upon request.

Received: 19 December 2024; Accepted: 20 June 2025;
Published online: 12 July 2025

References

1. Levitus, S. J. et al. World ocean heat content and thermosteric sea level change (0-2000m), 1955-2010. *Geophys. Res. Lett.* **39**, L10603 (2012).
2. Trenberth, K. E., Fasullo, J. T. & Balmaseda, M. A. Earth's energy imbalance. *J. Clim.* **27**, 3129–3144 (2014).
3. Roemmich, D. et al. Unbated planetary warming and its ocean structure since 2006. *Nat. Clim. Change* **5**, 240–245 (2015).
4. Cheng, L., Abraham, J., Hausfather, Z. & Trenberth, K. E. How fast are the oceans warming? *Science* **363**, 128–129 (2019).
5. Li, Z., England, M. H. & Groeskamp, S. Recent acceleration in global ocean heat accumulation by mode and intermediate waters. *Nat. Commun.* **14**, 6888 (2023).
6. Hanawa, K., & Talley, L. in *Ocean Circulation and Climate* (eds Siedler, G., Church, J. & Gould, J.) Ch. 5.4 (Academic Press, 2001).
7. Bingham, F. M. Formation and spreading of subtropical mode water in the North Pacific. *J. Geophys. Res. Oceans* **97**, 11177–11189 (1992).
8. Yasuda, T. & Hanawa, K. Decadal changes in the mode waters in the midlatitude North Pacific. *J. Phys. Oceanogr.* **27**, 858–870 (1997).
9. Oka, E. & Qiu, B. Progress of North Pacific mode water research in the past decade. *J. Oceanogr.* **68**, 5–20 (2012).
10. Häkkinen, S., Rhines, P. B. & Worthen, D. L. Heat content variability in the North Atlantic Ocean in ocean reanalyses. *Geophys. Res. Lett.* **42**, 2901–2909 (2015).
11. Gao, L., Rintoul, S. R. & Yu, W. D. Recent wind-driven change in Subantarctic Mode Water and its impact on ocean heat storage. *Nat. Clim. Change* **8**, 58–63 (2018).
12. McPhaden, M. J., Zebiak, S. E. & Glantz, M. H. ENSO as an integrating concept in earth science. *Science* **314**, 1740–1745 (2006).
13. Chavez, F. P. et al. Biological and chemical consequences of the 1997-1998 El Niño in central California waters. *Prog. Oceanogr.* **54**, 205–232 (2002).
14. Iizumi, T. et al. Impacts of El Niño Southern Oscillation on the global yields of major crops. *Nat. Commun.* **5**, 3712 (2014).
15. Patricola, C. M., Saravanan, R. & Chang, P. The impact of the El Niño – Southern Oscillation and Atlantic Meridional Mode on seasonal Atlantic tropical cyclone activity. *J. Clim.* **27**, 5311–5328 (2014).
16. Vicente-Serrano, S. M. et al. A multiscalar global evaluation of the impact of ENSO on droughts. *J. Geophys. Res. Atmos.* **116**, D20109 (2011).
17. Ward, P. J. et al. Strong influence of El Niño Southern Oscillation on flood risk around the world. *Proc. Natl Acad. Sci. USA* **111**, 15659–15664 (2014).
18. Jin, F. F. An equatorial ocean recharge paradigm for ENSO. Part I: conceptual model. *J. Atmos. Sci.* **54**, 811–829 (1997).
19. Li, X., Yu, J.-Y. & Ding, R. El Niño- La Niña asymmetries in the changes of ENSO complexities and dynamics since 1990. *Geophys. Res. Lett.* **51**, e2023GL106395 (2024).
20. Chiang, J. C. H. & Vimont, D. J. Analogous Pacific and Atlantic meridional modes of tropical atmosphere–ocean variability [Dataset]. *J. Clim.* **17**, 4143–4158 (2004).
21. Vimont, D. J., Battisti, D. S. & Hirst, A. C. Footprinting: a seasonal connection between the tropics and mid-latitudes. *Geophys. Res. Lett.* **28**, 3923–3926 (2001).
22. Yu, J. -Y. & Kim, S. T. Relationships between extratropical sea level pressure variations and the central Pacific and eastern Pacific types of ENSO. *J. Clim.* **24**, 708–720 (2011).

23. Yu, J.-Y., Wang, X., Yang, S., Paek, H., & Chen, M. in *Climate Extremes: Patterns and Mechanisms* (eds Simon Wang, S. -Y., Yoon, J.-H., Funk, C. C. & Gillies, R. R.) Ch. 1 (Wiley, 2017).
24. Toyoda, T. et al. Interannual variability of North Pacific eastern subtropical mode water formation in the 1990s derived from a 4-dimensional variational ocean data assimilation experiment. *Dyn. Atmos. Oceans* **51**, 1–25 (2011).
25. Wang, J., Liu, L. L., Lin, Y. F., Yu, J. Y. & Wang, F. A see-saw of subduction rate in the North Pacific western and eastern subtropical mode water formation areas induced by the Aleutian low. *Geophys. Res. Lett.* **51**, e2024GL110837 (2024).
26. McCreary, J. P. & Lu, P. Interaction between the subtropical and equatorial ocean circulations: the subtropical cell. *J. Phys. Oceanogr.* **24**, 466–497 (1994).
27. Gu, D. & Philander, S. G. H. Interdecadal climate fluctuations that depend on exchanged between the tropics and extratropics. *Science* **275**, 805–807 (1997).
28. Huang, R. X. & Wang, Q. Interior communication from the subtropical to the tropical oceans. *J. Phys. Oceanogr.* **31**, 3538–3550 (2002).
29. McPhaden, M. J. & Zhang, D. X. Slowdown of the meridional overturning circulation in the upper Pacific Ocean. *Nature* **415**, 603–608 (2002).
30. Katsura, S. Properties, formation, and dissipation of the North Pacific Eastern Subtropical Mode Water and its impact on interannual spiciness anomalies. *Prog. Oceanogr.* **162**, 120–131 (2018).
31. Yu, J. Y. & Fang, S. W. The distinct contributions of the seasonal footprinting and charged-discharged mechanisms to ENSO complexity. *Geophys. Res. Lett.* **45**, 6611–6618 (2018).
32. Fang, S. & Yu, J.-Y. A control of ENSO transition complexity by tropical Pacific mean SSTs through tropical-subtropical interaction. *Geophys. Res. Lett.* **47**, e2020GL08793 (2020).
33. Stuecker, M. F. et al. Revisiting ENSO/Indian ocean dipole phase relationships. *Geophys. Res. Lett.* **44**, 2481–2492 (2017).
34. Zhang, W. J., Jiang, F., Stuecker, M. F., Jin, F. F. & Timmermann, A. Spurious North Tropical Atlantic precursors to El Nino. *Nat. Commun.* **12**, 3096 (2021).
35. Hosoda, S., Xie, S. P., Takeuchi, K. & Nonaka, M. Eastern North Pacific subtropical mode water in a general circulation model: formation mechanism and salinity effects. *J. Geophys. Res.* **106**, 19671–19681 (2001).
36. Toyoda, T., Awaij, T., Ishikawa, Y. & Nakamura, T. Preconditioning of winter mixed layer in the formation of North Pacific eastern subtropical mode water. *Geophys. Res. Lett.* **31**, L17206 (2004).
37. Toyama, K., Iwasaki, A. & Suga, T. Interannual variation of annual subduction rate in the North Pacific estimated from a gridded Argo product. *J. Phys. Oceanogr.* **45**, 2276–2293 (2015).
38. Yeh, S. W., Wang, X., Wang, C. & Dewitte, B. On the relationship between the North Pacific climate variability and central Pacific El Niño. *J. Clim.* **28**, 663–677 (2015).
39. Ding, R. et al. Linking the North American dipole to the Pacific Meridional Mode. *J. Geophys. Res. Atmos.* **124**, 3020–3034 (2019).
40. Qiu, B. & Huang, R. X. Ventilation of the North Atlantic and North Pacific: subduction versus obduction. *J. Phys. Oceanogr.* **25**, 2374–2390 (1995).
41. Liu, L. & Huang, R. X. The global subduction/obduction rates: their interannual and decadal variability. *J. Clim.* **25**, 1096–1115 (2012).
42. Sasaki, Y. N., Schneider, N., Maximenko, N. & Lebedev, K. Observational evidence for propagation of decadal spiciness anomalies in the North Pacific. *Geophys. Res. Lett.* **37**, L07708 (2010).
43. Fukumori, I., Lee, T., Cheng, B. & Menemenlis, D. The origin, pathway, and destination of Niño 3 water estimated by a simulated passive tracer and its adjoint. *J. Phys. Oceanogr.* **34**, 582–604 (2004).
44. Capotondi, A., Alexander, M. A., Deser, C. & McPhaden, M. J. Anatomy and decadal evolution of the Pacific subtropical-tropical cells (STCs). *J. Clim.* **18**, 3739–3758 (2005).
45. Schott,F. A., Stramma, L., Wang, W., Giese, B. S., & Zantopp, R. Pacific subtropical cell variability in the SODA2.0.2/3 assimilation. *Geophys. Res. Lett*. https://doi.org/10.1029/2008GL033757 (2008)
46. Capotondi, A. et al. Mechanisms of tropical Pacific decadal variability. *Nat. Rev. Earth Environ.* **4**, 754–769 (2023).
47. Okumura, Y. M., DiNezio, P. & Deser, C. Evolving impacts of multiyear La Niña events on atmospheric circulation and U.S. drought. *Geophys. Res. Lett.* **44**, 11614–11623 (2017).
48. Iwakiri, T. & Watanabe, M. Multiyear La Niña impact on summer temperature over Japan. *J. Meteorol. Soc. Jpn. Ser. II* **98**, 1245–1260 (2020).
49. Anderson, W. et al. Multiyear La Niña events and multiseason drought in the horn of Africa. *J. Hydrometeorol.* **24**, 119–131 (2023).
50. Zhu, T. & Yu, J.-Y. A shifting tripolar pattern of Antarctic sea ice concentration anomalies during multi-year La Niña events. *Geophys. Res. Lett.* **49**, e2022GL101217 (2022).
51. Zhu, T. & Yu, J.-Y. Distinguishing impacts on winter temperatures in northern mid-to-high latitude continents during multi-year and single-year La Nina events: a modeling study. *J. Clim.* **37**, 3943–3958 (2024).
52. Yu, J.-Y., Kao, H.-Y. & Lee, T. Subtropics-related interannual sea surface temperature variability in the central Pacific. *J. Clim.* **23**, 2869–2884 (2010).
53. Fang, S. & Yu, J.-Y. Contrasting transition complexity between El Niño and La Niña: observations and CMIP5/6 models. *Geophys. Res. Lett.* **47**, e2020GL088926 (2020).
54. Ding, R. et al. Multi-year El Niño events tied to the North Pacific Oscillation. *Nat. Commun.* **13**, 3871 (2022).
55. Kim, J. W. & Yu, J. Y. Single- and multi-year ENSO events controlled by pantropical climate interactions. *npj Clim. Atmos. Sci.* **5**, 88 (2022).
56. Kim, J. W., Yu, J. Y. & Tian, B. J. Overemphasized role of preceding strong El Nino in generating multi-year La Nina events. *Nat. Commun.* **14**, 6790 (2023).
57. Li, X., Yu, J.-Y., Ding, R. Q., Hu, J. Y. & Tuo, P. F. Asymmetric efficacies between warm and cold Pacific Meridional Modes in inducing ENSO. *Geophys. Res. Lett.* **51**, e2024GL108924 (2024).
58. Jiang, F., Zhang, W., Boucharel, J. & Jin, F. F. Tropical origins of the Pacific Meridional Mode associated with the nonlinear interaction of ENSO with the annual cycle. *Geophys. Res. Lett.* **50**, e2023GL106225 (2023).
59. Chakravorty, S. et al. Testing the trade wind charging mechanism and its influence on ENSO variability. *J. Clim.* **33**, 7391–7411 (2020).
60. McPhaden, M. J. Tropical Pacific Ocean heat content variations and ENS persistence barriers. *Geophys. Res. Lett.* **30**, 1480 (2003).
61. Izumo, T., Lengaigne, M., Vialard, J., Suresh, I. & Planton, Y. On the physical interpretation of the lead relation between warm water volume and the El Niño Southern Oscillation. *Clim. Dyn.* **52**, 2923–2942 (2019).
62. Cheng, L. et al. Improved estimates of ocean heat content from 1960 to 2015. *Sci. Adv.* **3**, e1601545 (2017).
63. Good, S. A., Martin, M. J. & Rayner, N. A. EN4: quality controlled ocean temperature and salinity profiles and monthly objective analyses with uncertainty estimates. *J. Geophys. Res. Oceans* **18**, 6704–6716 (2013).
64. Carton, J. A., Chepurin, G. A. & Chen, L. SODA3: a new ocean climate reanalysis. *J. Clim.* **31**, 6967–6983 (2018).
65. Behringer, D., & Xue, Y. Evaluation of the global ocean data assimilation system at NCEP: the Pacific Ocean. In *Eighth Symposium on Integrated Observing and Assimilation Systems for Atmosphere, Oceans, and Land Surface* (American meteorological society, 2004).
66. Hautala, S. L. & Roemmich, D. H. Subtropical mode water in the Northeast Pacific basin. *J. Geophys. Res.* **103**, 13,055–13,066 (1998).
67. Huang, B. et al. Extended reconstructed sea surface temperature, version 5 (ERSSTv5): upgrades, validations, and intercomparisons. *J. Clim.* **30**, 8179–8205 (2017).

68. Kobayashi, S. et al. The JRA-55 reanalysis: general specifications and basic characteristics. *J. Meteorol. Soc. Jpn. Ser. II* **93**, 5–48 (2015).
69. Kay, J. E. et al. The Community Earth System Model (CESM) large ensemble project: a community resource for studying climate change in the presence of internal climate variability. *Bull. Am. Meteorol. Soc.* **96**, 1333–1349 (2015).
70. DiNezio, P. N., Deser, C., Okumura, Y. & Karspeck, A. Predictability of 2-year La Niña events in a coupled general circulation model. *Clim. Dyn.* **49**, 4237–4261 (2017).
71. Wu, X., Okumura, Y. M. & DiNezio, P. N. 2019: what controls the duration of El Niño and La Niña events? *J. Clim.* **32**, 5941–5965 (2019).
72. Kim, J.-W. & Yu, J.-Y. Understanding reintensified multi-year El Niño events. *Geophys. Res. Lett.* **47**, e2020GL087644 (2020).
73. Kim, J.-W. & Yu, J.-Y. Evolution of subtropical Pacific-onset El Niño: How its onset location controls its decay evolution. *Geophys. Res. Lett.* **48**, e2020GL091345 (2021).
74. Fan, H. J., Wang, C. & Yang, S. Asymmetry between positive and negative phases of the Pacific Meridional Mode: a contributor to ENSO transition complexity. *Geophys. Res. Lett.* **50**, e2023GL104000 (2023).
75. Richter, I., Stuecker, M. F., Takahashi, N. & Schneider, N. Disentangling the North Pacific Meridional Mode from tropical Pacific variability. *npj Clim. Atmos. Sci.* **5**, 94 (2022).
76. Lin, Y. F. & Yu, J. Y. The role of the Indian Ocean in controlling the formation of multiyear El Ninos through subtropical ENSO dynamics. *J. Clim.* **37**, 385–401 (2024).
77. Ladd, C. & Thompson, L. Formation mechanisms for North Pacific central and eastern subtropical mode waters. *J. Phys. Oceanogr.* **30**, 88–887 (2000).
78. Ladd, C. & Thompson, L. Water mass formation in an isopycnal model of the North Pacific. *J. Phys. Oceanogr.* **32**, 2870–2881 (2001).
79. Suga, T., Motoki, K., Aoki, Y. & Macdonald, A. M. The North Pacific climatology of winter mixed layer and mode waters. *J. Phys. Oceanogr.* **34**, 3–22 (2004).
80. Guo, Y. Q., Lin, X. P., Wei, M., Liu, C. & Men, G. Decadal variability of North Pacific eastern subtropical mode water. *J. Geophys. Res. Oceans* **123**, 6189–6206 (2018).
81. de Boyer Montégut, C., Madec, G., Fischer, A. S., Lazar, A. & Iudicone, D. Mixed layer depth over the global ocean: an examination of profile data and a profile-based climatology. *J. Geophys. Res.* **109**, C12003 (2004).

Acknowledgements

This research is supported by the National Natural Science Foundation of China (No. 42222602 and 42376031), the National Key Research and Development Program of China under Grant 2022YFC3104305, Laoshan Laboratory (No. LSKJ202202601), and the Taishan Scholars Program of Shandong Province.

Author contributions

L.L.L. and J.-Y.Y. designed the study and drafted the manuscript. L.L.L. performed the analysis, generated figures and tables. All authors contributed to interpreting the results and revising the manuscript.

Competing interests

The authors declare no competing interests.

Additional information

Supplementary information The online version contains supplementary material available at https://doi.org/10.1038/s41612-025-01147-0.

Correspondence and requests for materials should be addressed to LingLing Liu or Jin-Yi Yu.

Supporting Information for

Linking North Pacific Eastern Subtropical Mode Water to ENSO: precursor signatures and subtropical cell pathways

LingLing Liu[1,2,3,*], Jin-Yi Yu[2,*], Fan Wang[1,3], Jianing Wang[1,3], Yong-Fu Lin[4]

[1]Key Laboratory of Ocean Observation and Forecasting and Key Laboratory of Ocean Circulation and Waves, Institute of Oceanology, Chinese Academy of Sciences, Qingdao, China

[2]Department of Earth System Science, University of California, Irvine, CA, USA

[3]Laboratory for Ocean Dynamics and Climate, Qingdao Marine Science and Technology Center, Qingdao, China

[4]Research Center for Critical Issues, Academia Sinica, Tainan, Taiwan

This file includes:

Figures S1-S16

Table S1

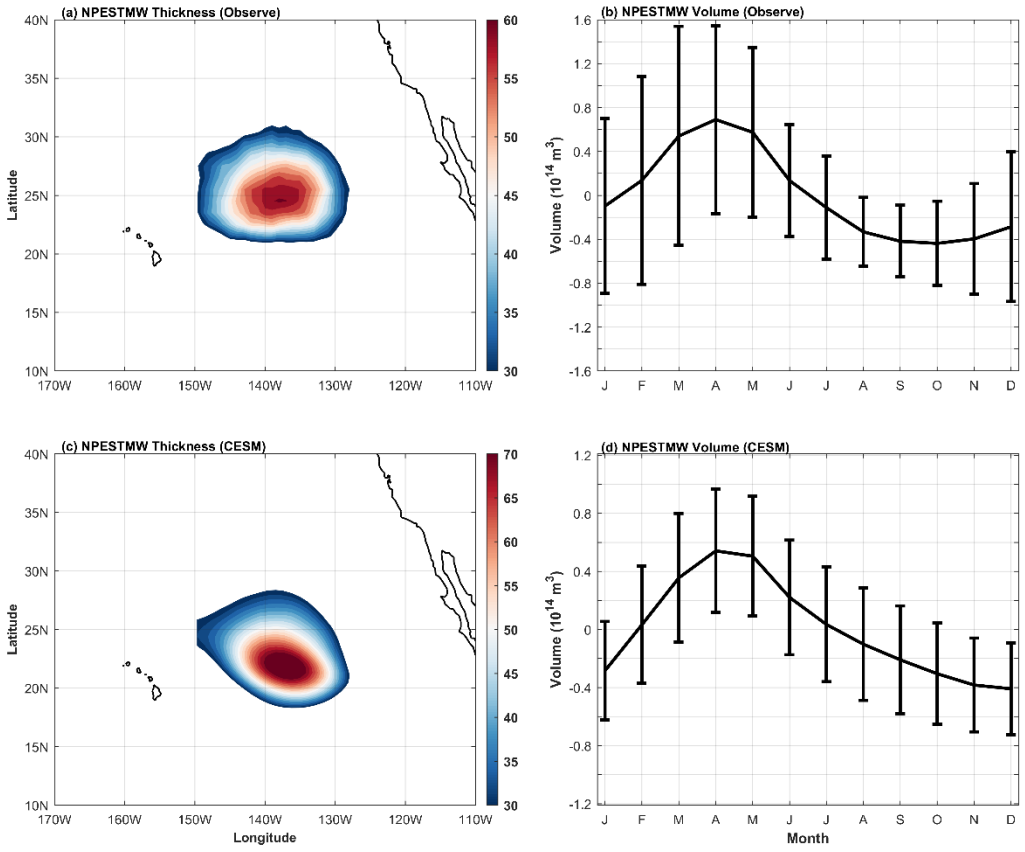

Fig.S1. Spatial and temporal characteristics of NPESTMW. a, The annual climatological thickness distribution of NPESTMW (unit: m). b, Seasonal cycle of NPESTMW volume, with the vertical bars indicating the standard deviation of NPESTMW volume among datasets. The observed results represent the ensemble mean from IAP, EN4, GODAS, and SODA3.4.2 datasets. c, Annual climatological thickness distribution of NPESTMW from CESM simulations (unit: m). d, Seasonal cycle of NPESTMW volume from CESM simulations. Vertical bars indicate the standard deviation of NPESTMW volume for each month.

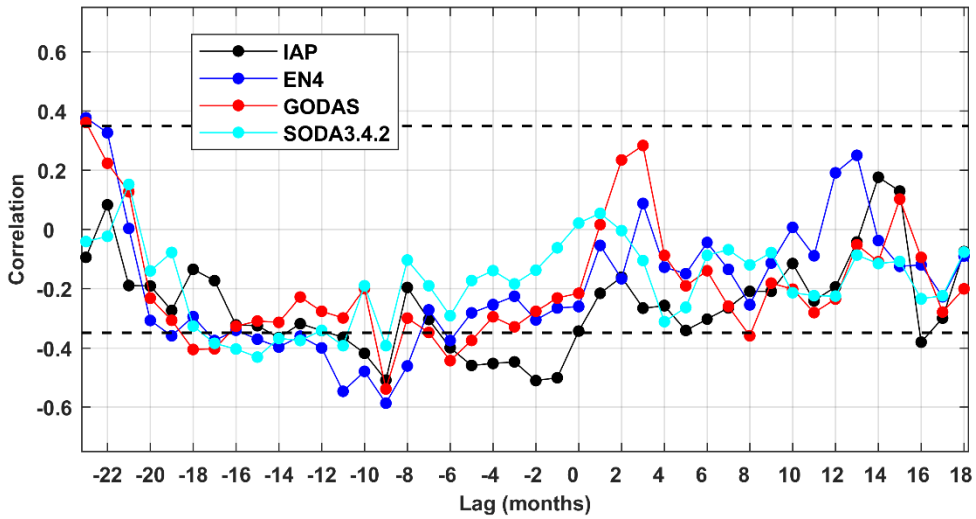

Fig.S2 Correlations between NPESTMW and ENSO. Lead-lag correlations between NPESTMW volume anomalies and November-December-January ONI for the period since 1991 for IAP (black), EN4 (blue), GODAS (red), and SODA3.4.2 (cyan), respectively. Dashed lines indicate the 95% confidence level. Positive lags denote ONI leading NPESTMW volume anomalies.

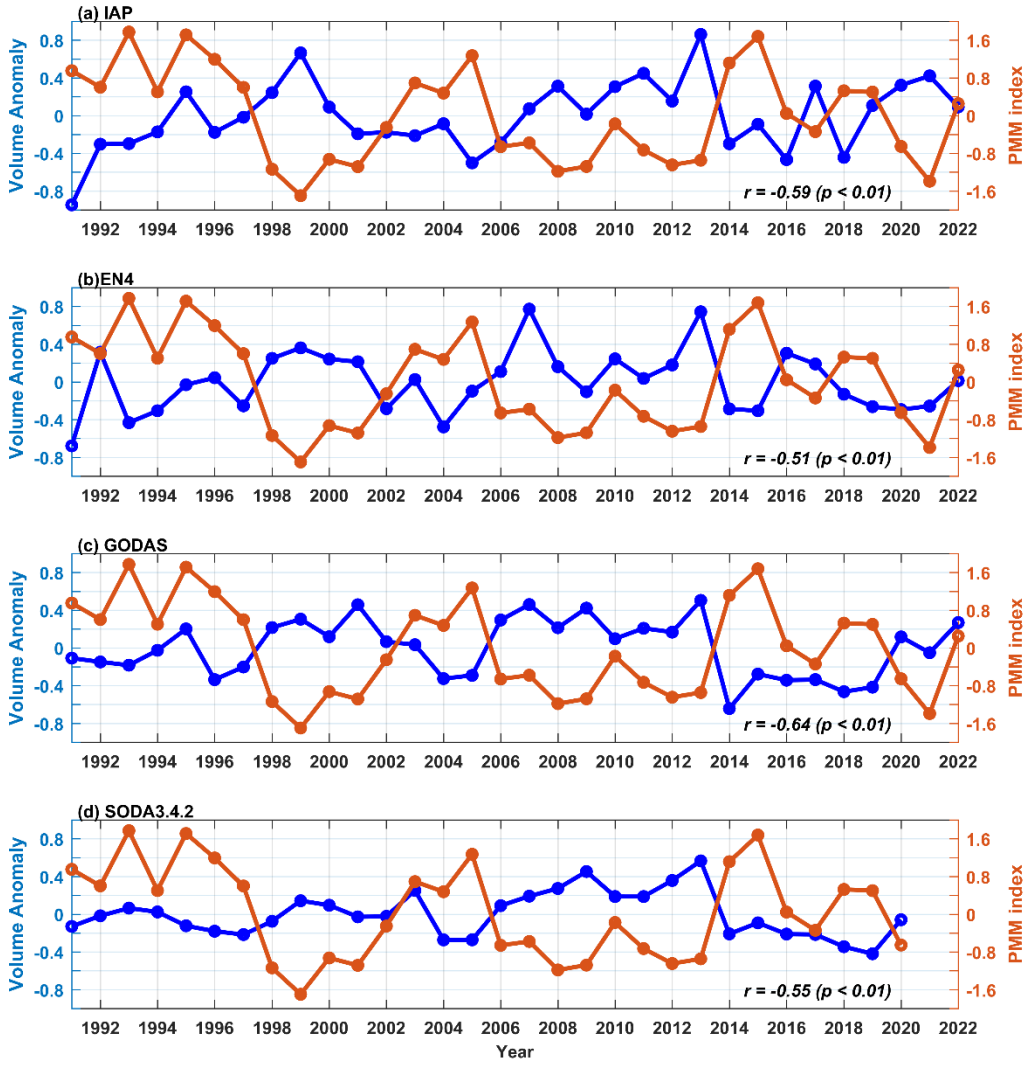

Fig.S3 Time series of NPESTMW volume anomalies and PMM. The time series of NPESTMW volume anomalies in March (IAP, EN4) / May (GODAS, SODA3.4.2) and normalized January-February-March PMM wind index (orange) for IAP (a), EN4 (b), GODAS (c), and SODA3.4.2 (d), respectively. The correlation coefficients are shown.

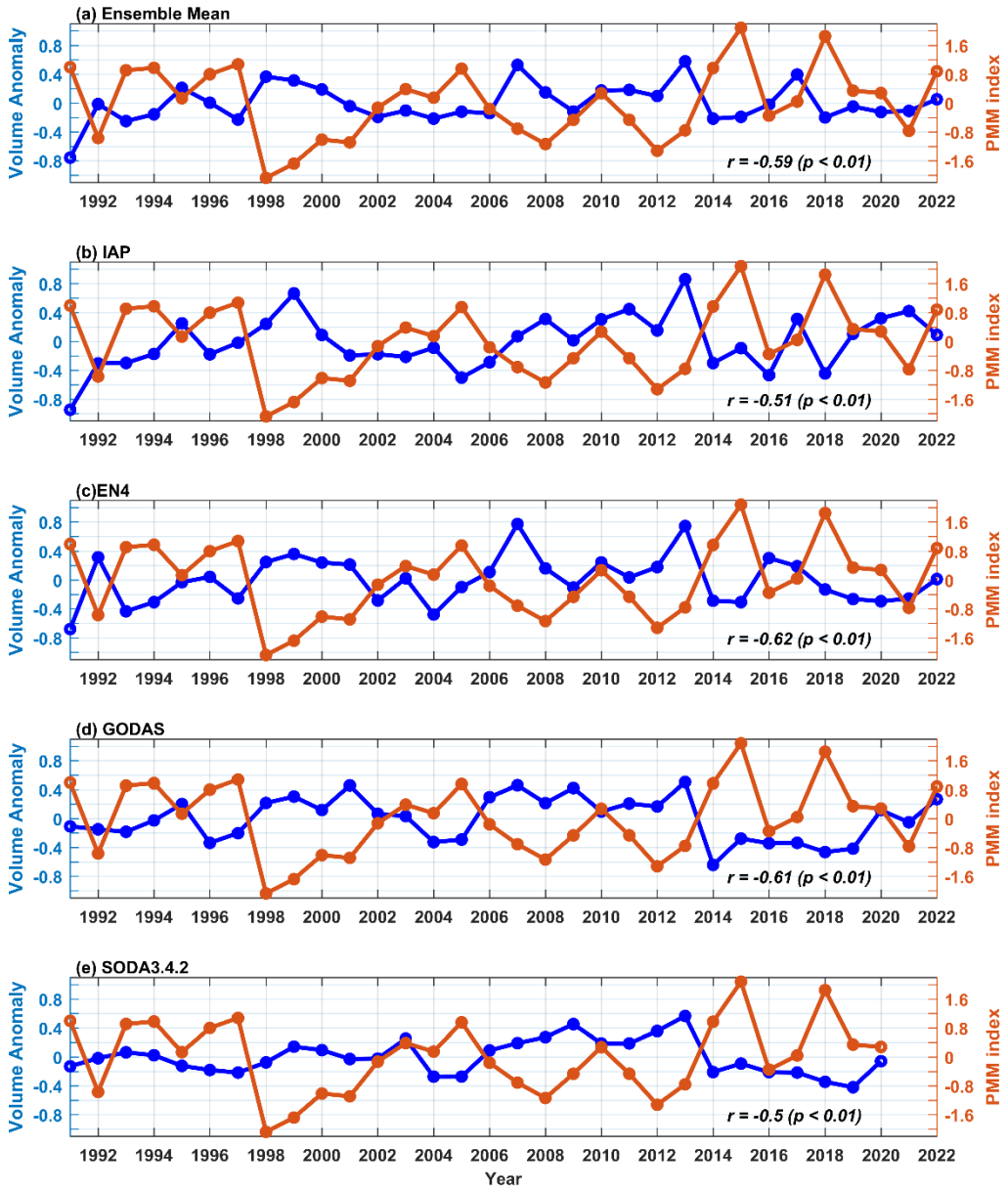

Fig.S4 Time series of NPESTMW volume anomalies and PMM. The time series of NPESTMW volume anomalies in March (the ensemble mean, IAP, and EN4) / May (GODAS, SODA3.4.2) and normalized January-February-March PMM SST index (orange) for the ensemble mean result (a), IAP (b), EN4 (c), GODAS (d), and SODA3.4.2 (f), respectively. The correlation coefficients are shown.

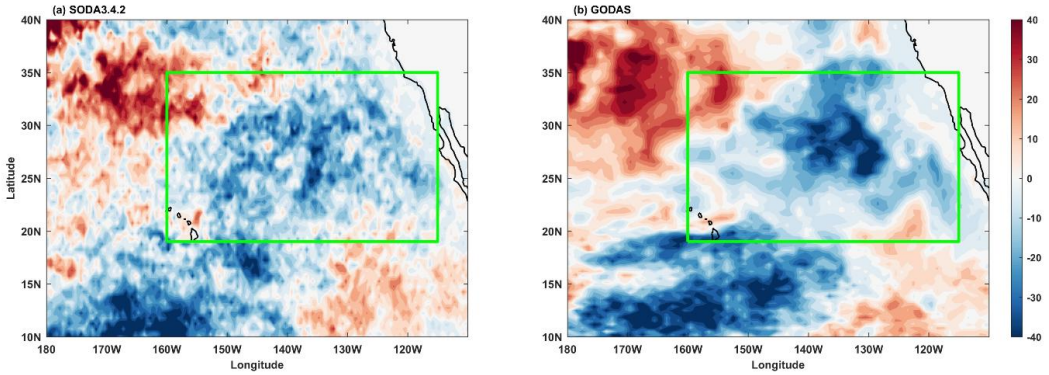

Fig.S5 Subduction rate. The subduction rate difference between positive PMM events and negative PMM events from SODA3.4.2 (a) and GODAS (b), with the unit of m yr^{-1}. The positive/negative PMM events are defined January-February-March PMM indices surpassing ±0.5 standard deviation. Green boxes denote the NPESTMW formation region.

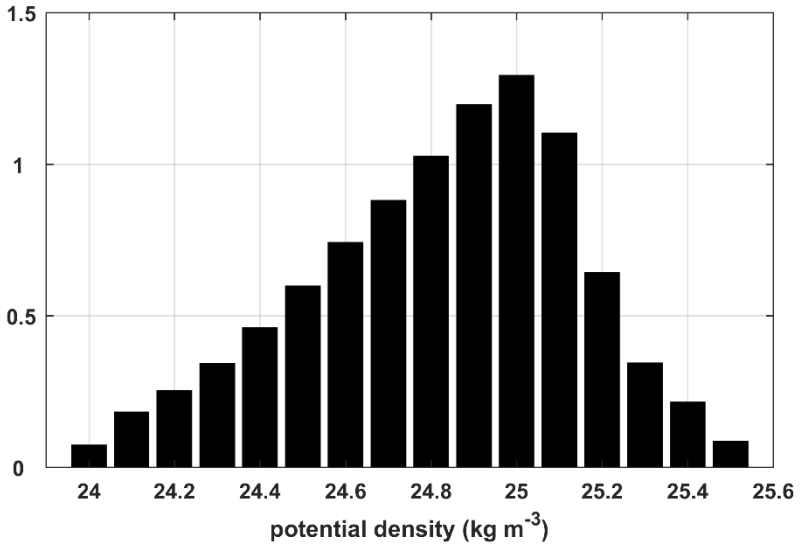

Fig. S6. NPESTMW distribution in potential density coordinate. The average of NPESTMW volume in each potential density range from IAP, EN4, GODAS, and SODA3.4.2.

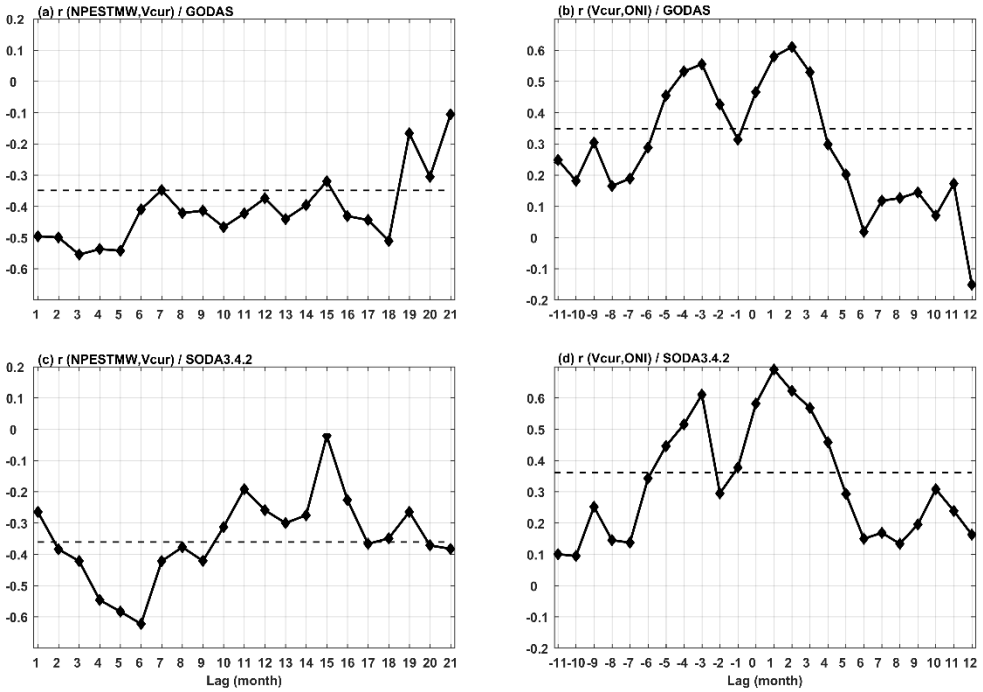

Fig.S7 The relationship between subtropical-tropical water exchange and NPESTMW / ENSO. Cross-correlation between March NPESTMW volume anomalies and meridional current anomalies, as a function of NPESTMW lead time for GODAS (a) and SODA3.4.2 (c). Cross-correlation between meridional current anomalies and November-December-January ONI, with negative lags indicating meridional current anomalies leading ONI for GODAS (b) and SODA3.4.2 (d). Dashed lines represent the 95% confidence levels.

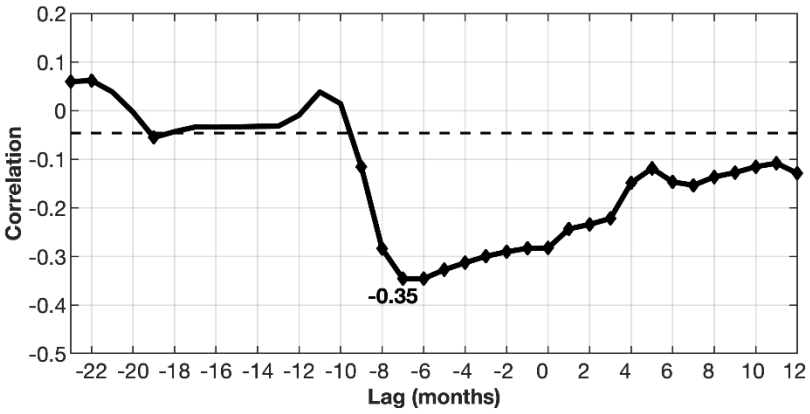

Fig.S8 Correlations between NPESTMW and ENSO in CESM simulations. Lead-lag correlations between NPESTMW volume anomalies and November-December-January ONI. Dashed lines indicate the 95% confidence level. Positive lags denote ONI leading NPESTMW volume anomalies.

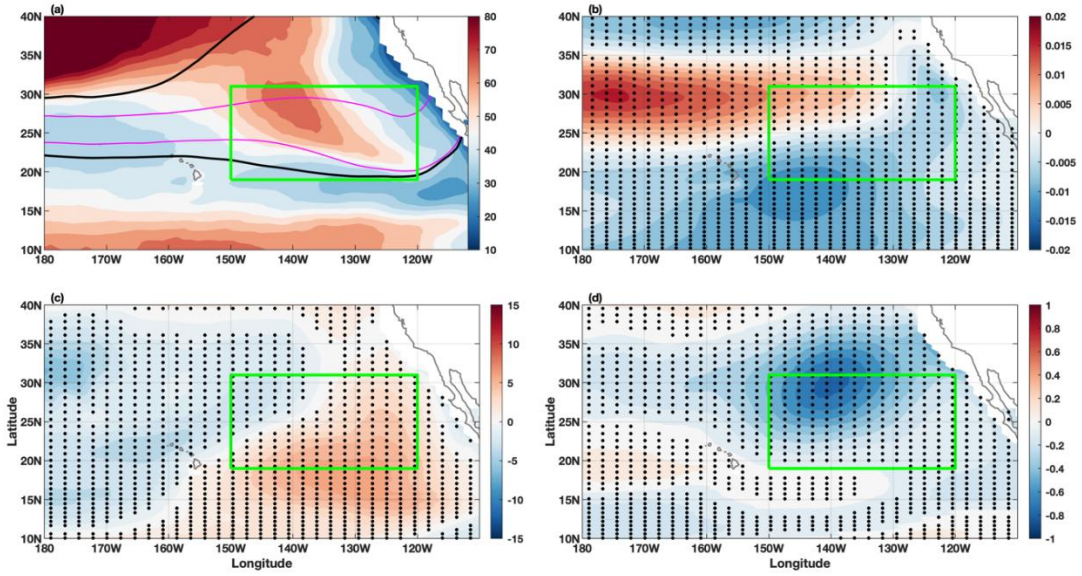

Fig.S9 NPESTMW formation region and PMM-related atmospheric forcings in CESM simulation. a, late-winter sea surface conditions: mixed layer depth (colors), sea surface potential density (black contours; 24 and 25.4 kg m^{-3}), and sea surface temperature (pink contours; 16°C and 22°C). b-d, Regression of normalized PMM index against (b) wind stress amplitude, (c) net downward surface heat flux (d), and (d) evaporation minus precipitation, averaged in March-April-May. Green boxes demote the NPESTMW formation region. Stipplings denote region significant at 95% confidence level (Student's t-test).

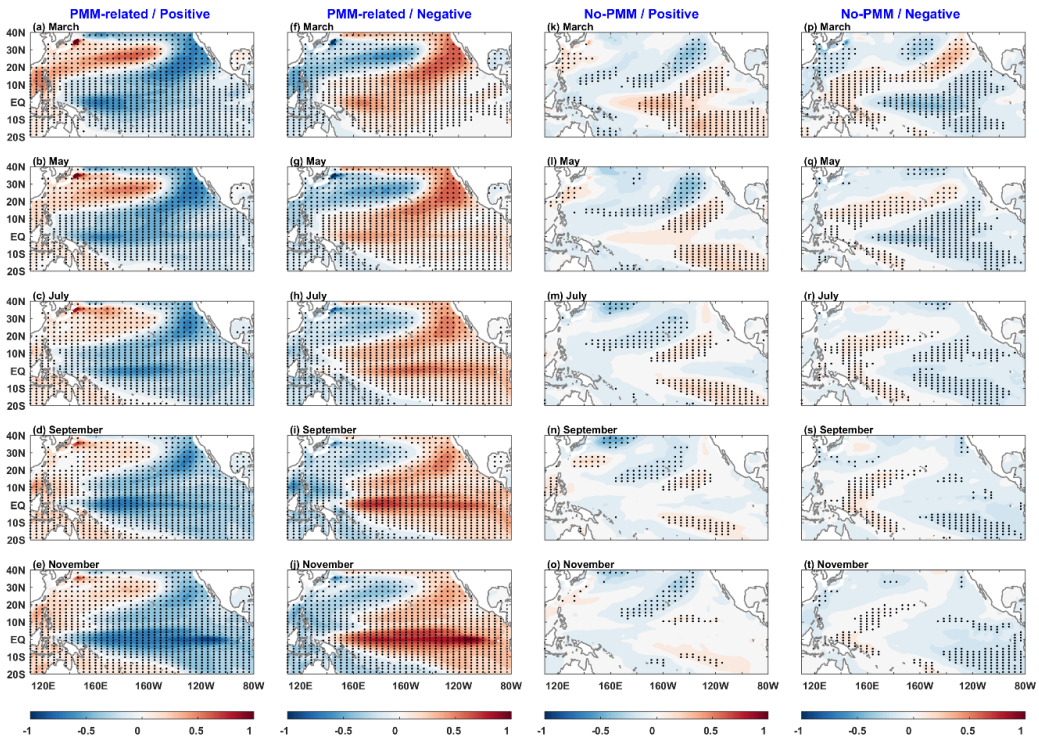

Fig.S10 Sea surface temperature (SST) evolution associated with NPESTMW volume anomalies. The SST anomaly during years with PMM-related (a-j) and no-PMM (k-t) positive (a-e, k-o) and negative (f-j, p-t) NPESTMW volume anomalies in CESM. NPESTMW anomaly years are defined by May NPESTMW volume anomalies exceeding ± 0.8 standard deviations. PMM-related events are identified when the March-April-May PMM index exceeds ± 0.5 standard deviations. In CESM simulations, 307 out of 389 NPESTMW positive anomalies years and 300 out of 392 negative anomaly years are PMM-related. Stipplings denote region significant at 95% confidence level (Student's t-test).

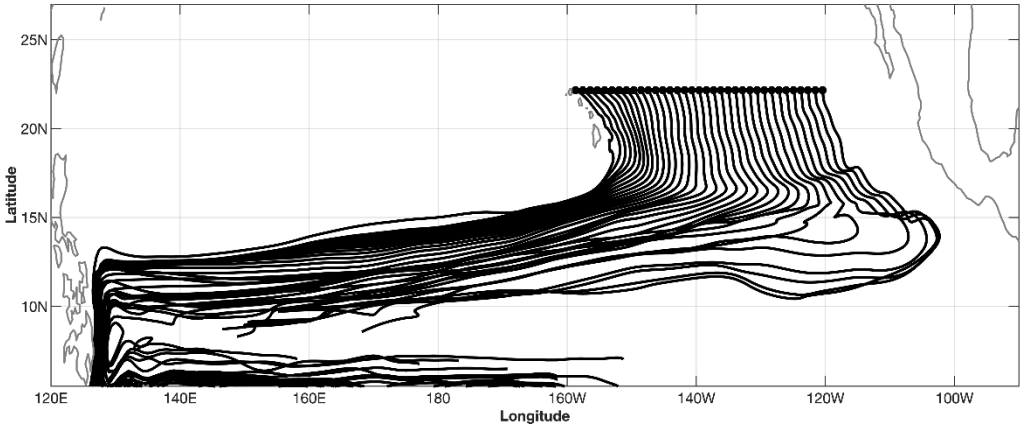

Fig.S11. Lagrangian trajectories in CESM over a 5-year period. Trajectories are initiated at 22.16°N and traced based on the climatological monthly velocity.

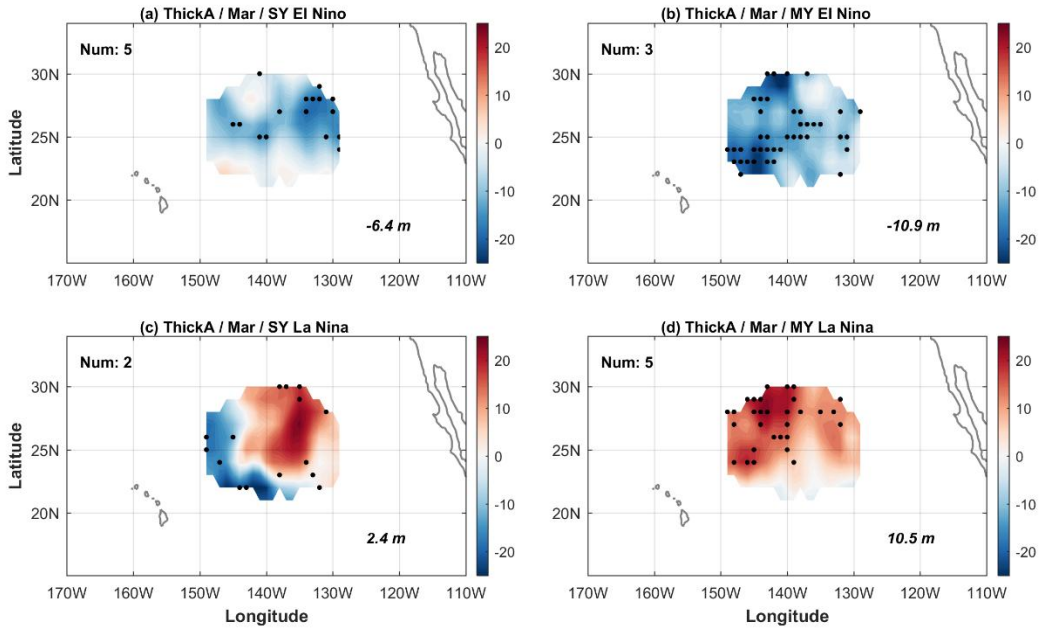

Fig.S12 Observed NPESTMW thickness anomalies during ENSO events. a-d, Composite NPESTMW thickness anomalies in March for single-year (a, c) and multi-year (b, d) El Niño (a, b) and La Niña (c, d) events. Insets: event frequency and region-averaged thickness anomalies. Stipplings denote region significant at 90% confidence level (Student's t-test).

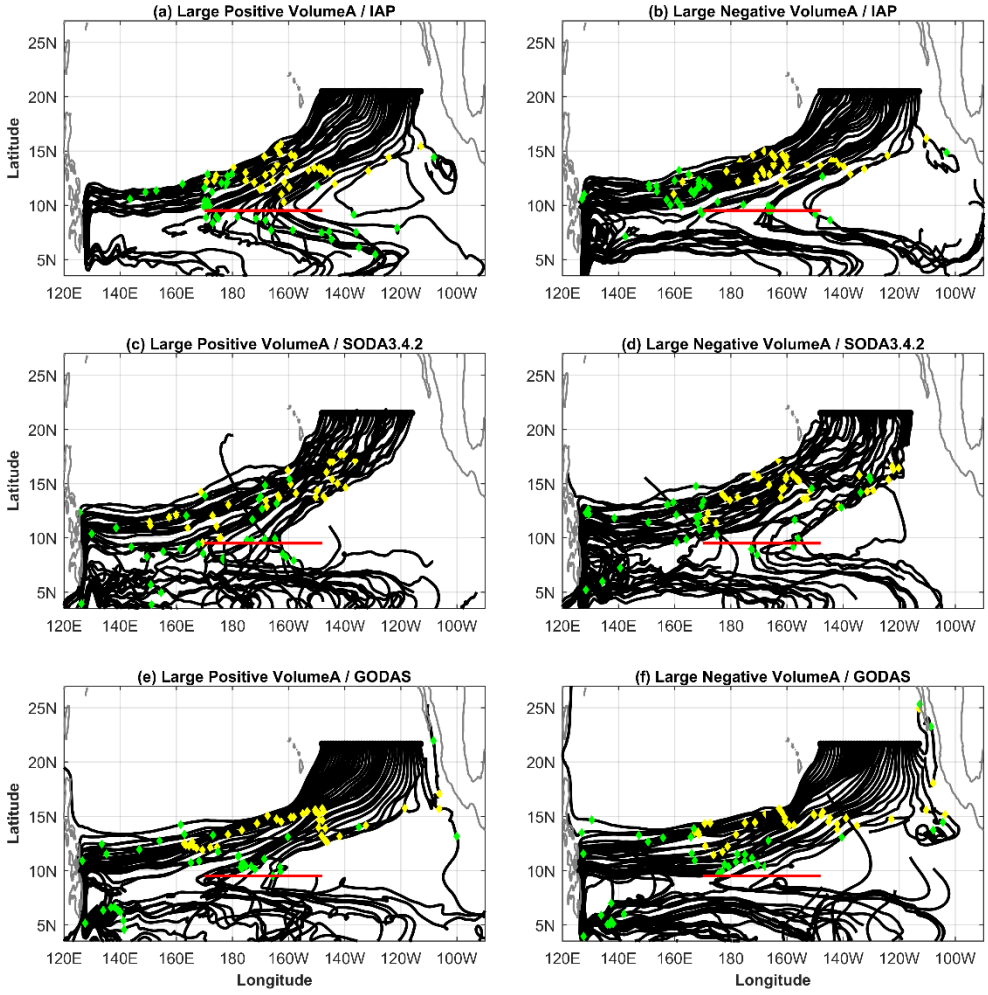

Fig.S13 Lagrangian trajectories during large NPESTMW volume anomaly events. The water mass trajectories identified from the Lagrangian tracing method based on the composite monthly velocity for NPESTMW large positive (a, c, e) and negative (b, d, f) anomaly years from IAP (a, b), SODA3.4.2 (c, d), and GODAS (e, f), respectively. The yellow and green diamonds represent the location of trajectories after tracing 2, and 3 years.

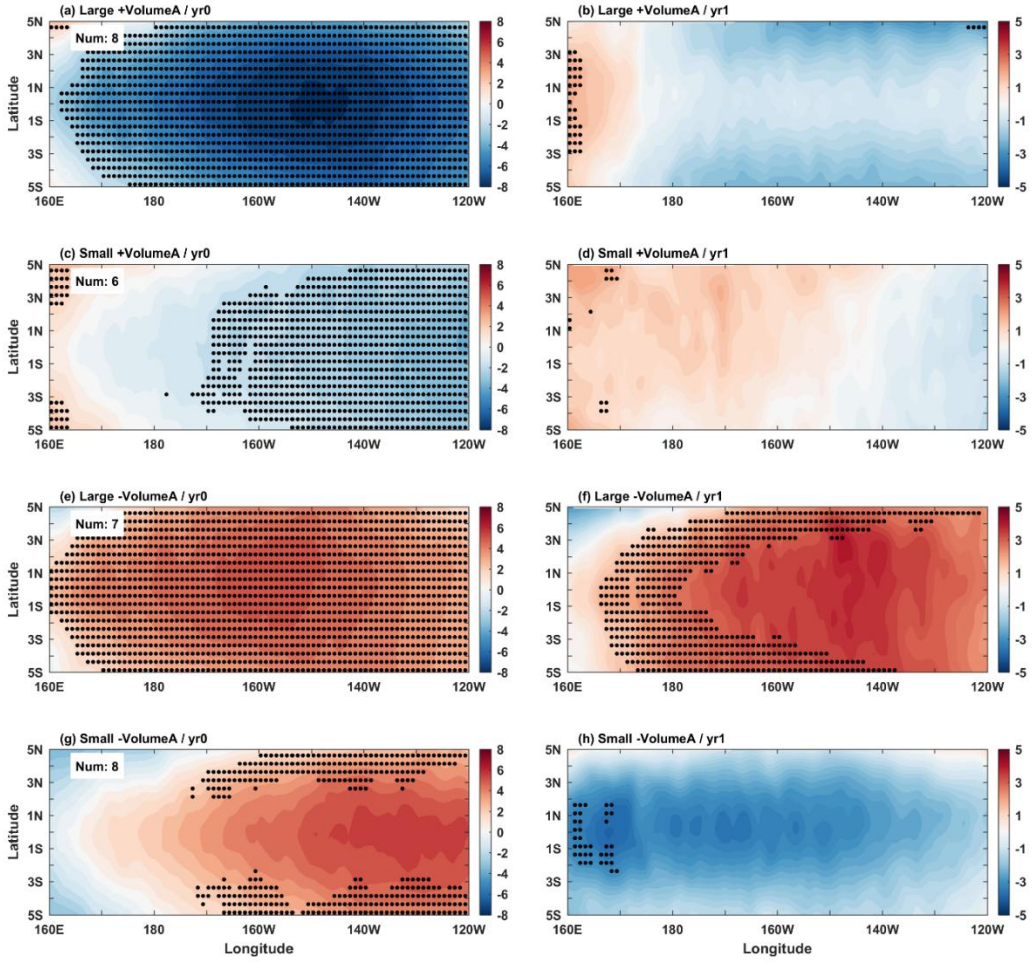

Fig.S14 Observed sea level anomalies during NPESTMW anomaly events. a-h, Composite sea level anomalies averaged from March to December during the first (a, c, e, g) and second (b, d, f, h) year for strong (a, b, e, f) and weak (c, d, g, h) NPESTMW anomaly years. Insets: Event frequency. Stipplings denotes region significant at 90% confidence level (Student's t-test).

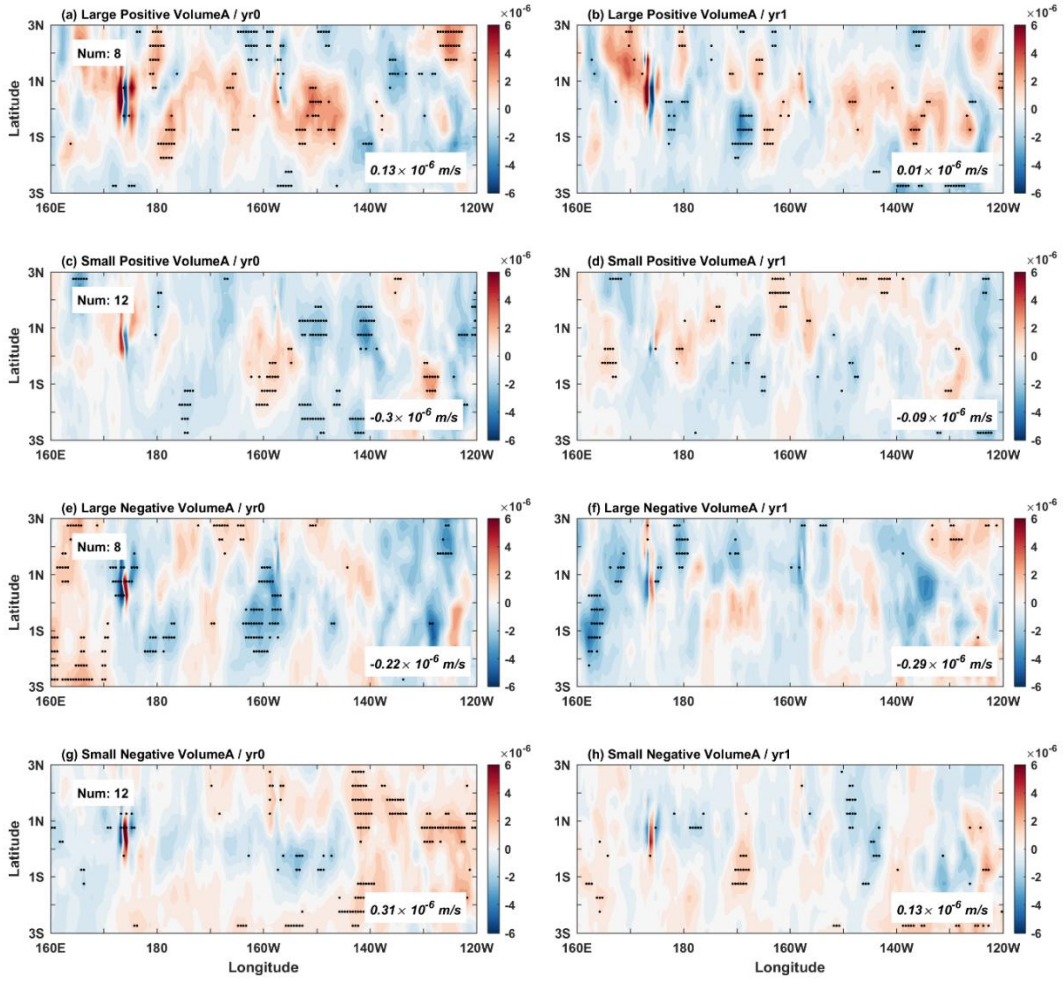

Fig.S15 Equatorial upwelling anomalies during NPESTMW anomaly events in SODA3.4.2. a-h, Composite equatorial upwelling averaged from March to December during the first (a, c, e, g) and second (b, d, f, h) year for strong (a, b, e, f) and weak (c, d, g, h) NPESTMW anomaly years. Insets: Event frequency and the mean equatorial upwelling anomalies (3°S-3°N, 170°W-120°W). Stipplings denote region significant at 90% confidence level (Student's t-test).

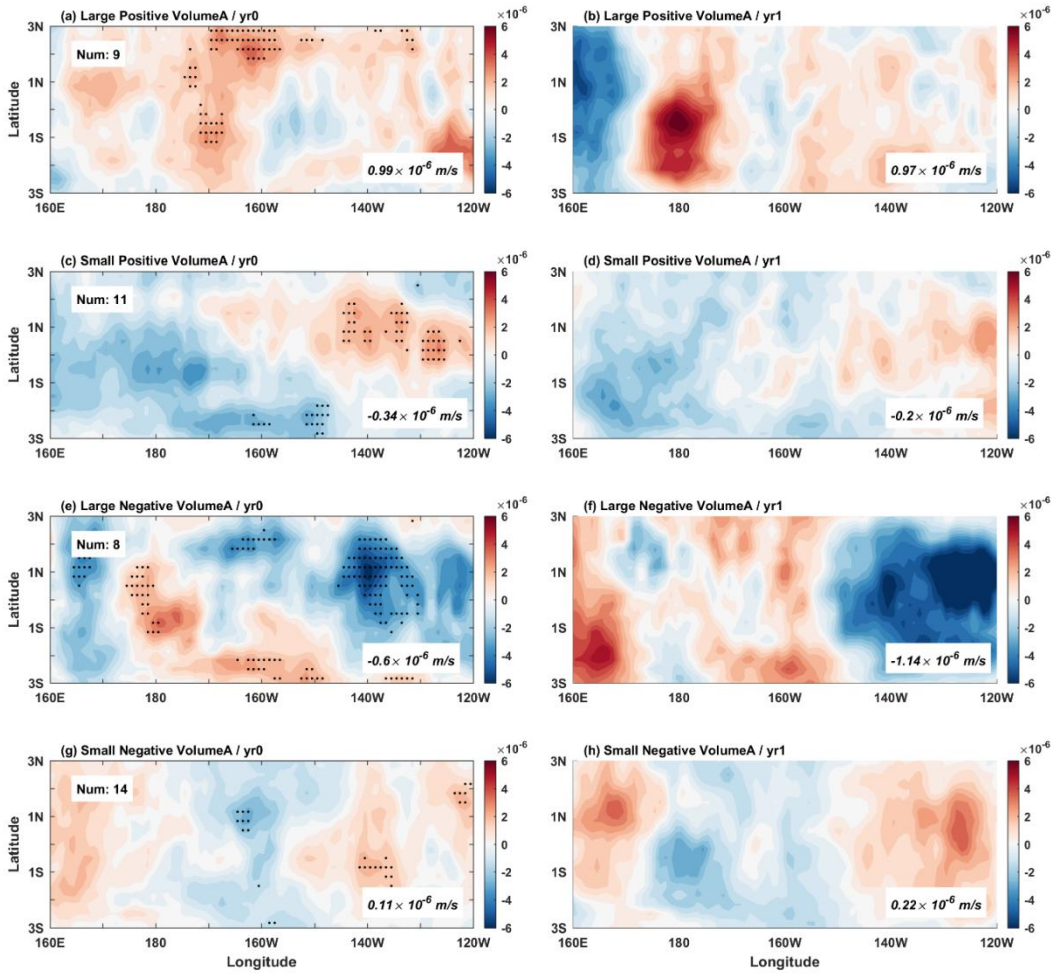

Fig.S16 Same as Fig.S15 but for GODAS.

Table S1. The large NPESTMW anomaly events and the preceding/subsequent ENSO events. Large NPESTMW anomaly is defined as the ensemble mean NPESTMW volume anomaly in March larger than ±0.6 standard deviations. PMM-related events are identified when the January-February-March PMM index exceeds ±0.5 standard deviations. Each ENSO event is labeled as EP (Eastern Pacific) or CP (Central Pacific) and SY (Single-Year) or MY (Multi-Year) based on its spatial and temporal characteristics.

Classification		Year	Preceded ENSO	Subsequent ENSO		
				ENSO	EP or CP	SY or MY
Positive NPESTMW events	PMM-related	1998	El Niño	La Niña	CP	MY
		1999	La Niña	La Niña	CP	MY
		2000	La Niña	La Niña	CP	SY
		2007	El Niño	La Niña	EP	MY
		2011	La Niña	La Niña	CP	SY
		2013	--	--	--	--
		2017	La Niña	La Niña	EP	SY
	No-PMM	1995	El Niño	La Niña	EP	MY
		2010	El Niño	La Niña	CP	MY
Negative NPESTMW events	PMM-related	1991	--	El Niño	CP	SY
		1993	--	--	--	--
		2014	--	El Niño	CP	MY
		2015	El Niño	El Niño	EP	SY
	No-PMM	1997	--	El Niño	EP	SY
		2002	--	El Niño	CP	MY
		2004	--	El Niño	CP	SY
		2018	La Niña	El Niño	EP	MY